**Atmospheric
Measurement
Techniques**

Measurements of tropospheric HO_2 and RO_2 by oxygen dilution modulation and chemical ionization mass spectrometry

R. S. Hornbrook[1,*], J. H. Crawford[2], G. D. Edwards[1,*], O. Goyea[1,**], R. L. Mauldin III[1,3], J. S. Olson[2], and C. A. Cantrell[1]

[1]Atmospheric Chemistry Division, National Center for Atmospheric Research, 1850 Table Mesa Drive, P.O. Box 3000, Boulder, CO, USA
[2]Atmospheric Sciences Division, Langley Research Center, NASA, Hampton, VA, USA
[3]Department of Physics, 00014 University of Helsinki, Helsinki, Finland
[*]now at: Department of Chemistry, Eastern Michigan University, Ypsilanti, MI, USA
[**]now at: United States Patent and Trademark Office, Department of Commerce, Alexandria, VA, USA

Abstract. An improved method for the measurement of hydroperoxy radicals (HO_2) and organic peroxy radicals (RO_2, where R is any organic group) has been developed that combines two previous chemical conversion/chemical ionization mass spectrometry (CIMS) peroxy radical measurement techniques. Applicable to both ground-based and aircraft platforms, the method provides good separation between HO_2 and RO_2, and frequent measurement capability with observations of both HO_2 and $HO_2 + RO_2$ amounts each minute. These improvements allow for analyses of measured $[HO_2]/[HO_2 + RO_2]$ ratios on timescales relevant to tropospheric photochemistry. By varying both [NO] and $[O_2]$ simultaneously in the chemical conversion region of the PeRCIMS (Peroxy Radical CIMS) inlet, the method exploits the changing conversion efficiency of RO_2 to HO_2 under different inlet $[NO]/[O_2]$ to selectively observe either primarily HO_2 or the sum of HO_2 and RO_2. Two modes of operation have been established for ambient measurements: in the first half of the minute, RO_2 radicals are measured at close to 100% efficiency along with HO_2 radicals (low $[NO]/[O_2] = 2.53 \times 10^{-5}$) and in the second half of the minute, HO_2 is detected while the majority of ambient RO_2 radicals are measured with low efficiency, approximately 15% (high $[NO]/[O_2] = 6.80 \times 10^{-4}$). The method has been tested extensively in the laboratory under various conditions and for a variety of organic peroxy radicals relevant to the atmosphere and the results of these tests are presented. The modified PeRCIMS instrument has been deployed successfully using the new measurement technique on a number of aircraft campaigns, including on the NSF/NCAR C-130 during the MIRAGE-Mex and NASA INTEX-B field campaigns in the spring of 2006. A brief comparison of the peroxy radical measurements during these campaigns to a photochemical box model indicates good agreement under tropospheric conditions where NO_x ($NO + NO_2$) concentrations are lower than 0.5 ppbV (parts per billion by volume).

1 Introduction

Peroxy radicals, including hydroperoxy radicals (HO_2) and organic peroxy radicals (RO_2, where R is any organic group) are important tropospheric photochemical species having a critical role in tropospheric ozone formation, as a reservoir for hydroxyl radicals (OH), and the primary source of gas-phase peroxides. In air masses with low NO_x ($NO + NO_2$), the dominant sinks for peroxy radicals are via self- and cross reactions, forming peroxides and other species (Tyndall et al., 2001; Hasson et al., 2003; Calvert et al., 2008). Where NO_x concentrations are higher, peroxy radicals efficiently convert NO into NO_2, regenerating OH. The resulting NO_2 can be photolyzed to generate O_3. At very high NO_x, production of HNO_3 from the reaction of OH with NO_2 dominates (Brasseur et al., 1999).

Presently-available techniques for observing RO_2 include chemical amplification (Green et al., 2006), chemical ionization mass spectrometry (CIMS) (Hanke et al., 2002; Cantrell et al., 2003a,b,c; Ren et al., 2005), and laser-induced
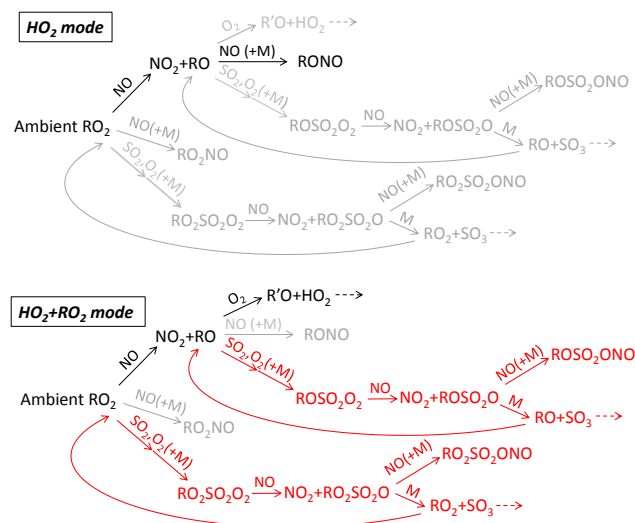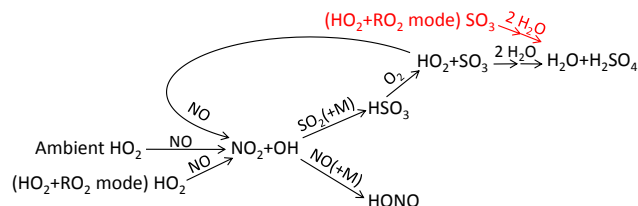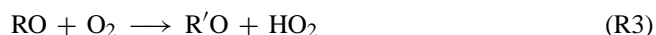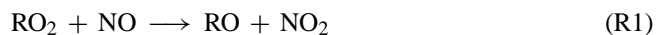
Scheme 1. PeRCIMS inlet RO$_2$ chemistry in the HO$_2$ mode and HO$_2$ + RO$_2$ mode. Reactions in black are known reactions (see text). Reactions in grey are deemed either unimportant or suppressed by competing reactions. Reactions in red show proposed chemistry based on inlet chemistry modeling (Sect. 3.2.3).

fluorescence (LIF) (Fuchs et al., 2008). Each of these techniques, including the method we present here, use similar chemical conversion schemes which provide a measurement of the sum of RO$_2$ rather than speciated RO$_2$. For a detailed comparison of all peroxy radical measurement techniques, the reader is directed to a review of OH and HO$_2$ measurements by Heard and Pilling (2003) and to Fuchs et al. (2008) for an updated overview. Although RO$_2$ speciation has not been achieved, observations of organic peroxy and hydroperoxy radicals are valuable components for understanding and modeling tropospheric photochemistry. Separate observations of [HO$_2$] and [HO$_2$ + RO$_2$] under photochemical timescales can improve our understanding of atmospheric processes involving VOCs and NO$_x$ and the partitioning that occurs between OH and HO$_2$ and between the hydro- and organic peroxy radical forms.

The method presented here builds on the previous work of this research group using the Peroxy Radical Chemical Ionization Mass Spectrometry (PeRCIMS) inlet (Edwards et al., 2003) by adding a dilution step similar to that described by Hanke et al. (2002). In all three techniques, [HO$_2$] and [HO$_2$ + RO$_2$] are measured independently by exploiting the competing chemistry that converts alkoxy (RO) radicals, formed in reactions of RO$_2$ with added NO in the inlet, into either HO$_2$ or alkyl nitrites via the following:

$$\text{RO}_2 + \text{NO} \longrightarrow \text{RO} + \text{NO}_2 \tag{R1}$$

$$\text{RO} + \text{NO} + M \longrightarrow \text{RONO} + M \tag{R2}$$

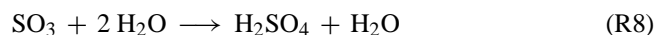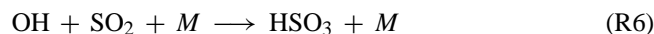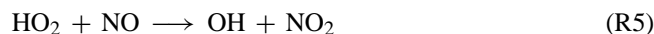$$\text{RO} + \text{O}_2 \longrightarrow \text{R}'\text{O} + \text{HO}_2 \tag{R3}$$

Scheme 2. PeRCIMS inlet HO$_2$ chemistry. Reactions in black are known reactions (see text). Reactions in red show proposed chemistry based on inlet chemistry modeling (Sect. 3.2.3).

$$\text{RO}_2 + \text{NO} + M \longrightarrow \text{RONO}_2 + M \tag{R4}$$

Here, Reaction (R3) requires that the RO radical has available α-hydrogen atoms that can be abstracted. For inlet conditions $k_3[\text{O}_2] > k_2[\text{NO}][M]$, there is increased likelihood for alkoxy radicals to react with O$_2$ to generate HO$_2$. Similarly, where $k_3[\text{O}_2] < k_2[\text{NO}][M]$, RO is more likely to form an alkyl nitrite via Reaction (R2). There can also be substantial formation of the alkyl nitrate via Reaction (R4) in competition with Reaction (R1), generally increasing in importance as the size of the R group increases. This RO$_2$ separation chemistry is shown in Scheme 1, along with additional reaction pathways that will be discussed in a later section.

Both ambient HO$_2$ radicals and HO$_2$ radicals formed in Reaction (R3) are converted into H$_2$SO$_4$ in the inlet through reactions with added NO and SO$_2$ via:

$$\text{HO}_2 + \text{NO} \longrightarrow \text{OH} + \text{NO}_2 \tag{R5}$$

$$\text{OH} + \text{SO}_2 + M \longrightarrow \text{HSO}_3 + M \tag{R6}$$

$$\text{HSO}_3 + \text{O}_2 \longrightarrow \text{HO}_2 + \text{SO}_3 \tag{R7}$$

$$\text{SO}_3 + 2\,\text{H}_2\text{O} \longrightarrow \text{H}_2\text{SO}_4 + \text{H}_2\text{O} \tag{R8}$$

$$\text{OH} + \text{NO} + M \longrightarrow \text{HONO} + M \tag{R9}$$

The formation of HSO$_3$ in Reaction (R6) leads to HO$_2$ being recycled in Reaction (R7), but this cycle is terminated by Reaction (R9). Therefore, the residence time in the neutral chemistry region and the ratio of [SO$_2$]/[NO] determines the competing chemistry of OH reactions with SO$_2$ and NO (Reactions R6 and R9), and thus the sulfuric acid yield, $\Delta[\text{H}_2\text{SO}_4]/[\text{HO}_2]_\text{o}$, from (Reactions R5–R8). A summary of the HO$_2$ conversion chemistry is shown in Scheme 2.

The method described by Edwards et al. (2003) involves varying [NO] in the chemical conversion region of the PeRCIMS inlet to either enhance or reduce the rate of Reaction (R2) and likewise the measurement sensitivity to organic peroxy radicals. The concentration of NO in the inlet is changed by adding either pure NO or a 3000 ppmV (parts per million by volume) mixture of NO in N$_2$ to the front injector of the inlet. To maintain a constant chain length of $\Delta[\text{H}_2\text{SO}_4]/[\text{HO}_2]_\text{o}$, inlet [SO$_2$] is simultaneously adjusted

by adding either pure SO$_2$ gas or a 1% mixture of SO$_2$ in N$_2$ to the front injector gas mixture. A serious drawback to this method is the time required to switch from HO$_2$ measurement to HO$_2$ + RO$_2$ measurement: on the order of 30 min to allow adequate time for the pure reagent gases to be flushed from the inlet. Using this method, the conversion efficiency of RO$_2$ into HO$_2$ (α_{RO_2}) is reported to be 0.10–0.15 using pure reagent gases and 0.80–0.90 using dilute reagent gas mixtures, giving an approximate sixfold separation between HO$_2$ and HO$_2$ + RO$_2$, but under timescales that are long in comparison to photochemistry and not ideal for aircraft measurements.

Using an inlet similar to the PeRCIMS inlet with the same conversion chemistry, Hanke et al. (2002) describe a CIMS method in which RO$_2$ is selectively measured by adjusting the O$_2$ concentration in the chemical conversion region to either enhance or reduce the rate of Reaction (R3). This is done by diluting the sample flow by 75% or more with either O$_2$ or N$_2$. A constant sample flow is maintained while the [NO]/[O$_2$] ratio in the inlet is increased or decreased. The authors reported α_{RO_2} values of 0.25–0.30 with N$_2$ dilution (HO$_2$ mode), and 0.90 with O$_2$ dilution (HO$_2$ + RO$_2$ mode), with measurements of both modes made approximately once per minute. While the reported one-minute measurement cycle is more appropriate for timescales relevant to photochemistry and airborne measurements, the separation between HO$_2$ and HO$_2$ + RO$_2$ is weaker in comparison to the method described by Edwards and colleagues. Additionally, there is an inherent loss in sensitivity caused by diluting the ambient sample to one quarter or less of the sample flow.

The method we present here is a combination of the two methods described above in which both [NO] and [O$_2$] are modulated in the inlet to generate a low [NO]/[O$_2$] measurement mode and a high [NO]/[O$_2$] measurement mode. By varying the inlet [O$_2$], the requirement for pure NO and SO$_2$ reagent gases is eliminated. Likewise, by adjusting the NO mixture flow rate, good separation can be achieved with only 50% dilution of the sample air. This enables independent [HO$_2$] and [HO$_2$ + RO$_2$] observations to be made each minute and provides better measurement separation than with dilution alone by allowing for [NO]/[O$_2$] ratios in the two modes that differ by a greater amount. Although two inlet conditions have been established for observations of ambient peroxy radicals via the new method, the modified PeRCIMS inlet has been tested extensively in the laboratory under a wide range of [NO]/[O$_2$] conditions to characterize the oxygen dilution modulation method under a variety of conditions and for a large selection of common organic peroxy radicals.

Table 1. Standard Ambient PeRCIMS Operating Conditions.

| Mode	HO$_2$ + RO$_2$	HO$_2$
Diluent	O$_2$	N$_2$
Sampled Air:Diluent	1:1	1:1
Inlet NO mixing ratio	15.0 ppmV	67.5 ppmV
Inlet SO$_2$ mixing ratio	400 ppmV	1800 ppmV
O$_2$ mixing ratio	58.0%	10.1%
Inlet [NO]/[O$_2$]	2.53×10^{-5}	6.80×10^{-4}
	1.22 ± 0.08	0.17 ± 0.04
Δ[H$_2$SO$_4$]/[HO$_2$]$_0$ yield	5.5	5.5
Reaction time (neutral region)	0.124 s ($P_{amb} = 1.0 \times 10^5$ Pa)	
	0.276 s ($P_{amb} = 5.0 \times 10^4$ Pa)	
Reaction time (ion region)	0.276 s ($P_{amb} = 1.0 \times 10^5$ Pa)	
	0.552 s ($P_{amb} = 5.0 \times 10^4$ Pa)	
Inlet pressure	Variable, but typically held at 2×10^4 Pa	
Chamber pressure	Differentially pumped, from 1.0 to $< 1.0 \times 10^{-3}$ Pa	
Detection method	Quadrupole mass spectrometry of HSO$_4^-$	
Detection limit	2 pptV	
Electronic noise	<1% of radical signal	
Signal/background ratio	>2:1 for most ambient conditions	

2 Experimental

2.1 Principles of operation

Shown in Fig. 1, the modified PeRCIMS instrument utilizes a technique in which ambient HO$_2$ and RO$_2$ are chemically converted to HSO$_4^-$ ions that are then detected quantitatively by mass spectrometry. With the exception of the diluent region, the basic components of the instrument are similar to that described by Edwards et al. (2003), and thus only a summary is presented here.

2.2 Dilution

The primary modification to the instrumentation is the addition of a dilution region to the intake of the inlet (Fig. 1, inset). Sample air containing peroxy radicals is drawn through a 2.7-mm diameter orifice into the dilution region of the PeRCIMS inlet where either N$_2$ or O$_2$ (UHP, United States Welding) is added. For ambient peroxy radical observations, two measurement modes have been established and the details for these are listed in Table 1. In the HO$_2$ + RO$_2$ mode, sampled air is diluted by half with O$_2$, and in the HO$_2$ mode, sampled air is diluted by half with N$_2$. With ambient air at standard pressure and the neutral chemistry region pressure controlled at 2.00×10^4 Pa, the flow of gas from the dilution region of the inlet into the neutral chemistry region is 2.32 standard liters per minute (SLPM). Thus, to generate a 1:1 ratio of diluent to sample air, diluent O$_2$ and N$_2$ flow rates are computer-controlled using mass flow controllers (MKS) at 1.16 SLPM at sea level and adjusted to maintain a 1:1 ratio of diluent to sampled air for measurements at lower ambient
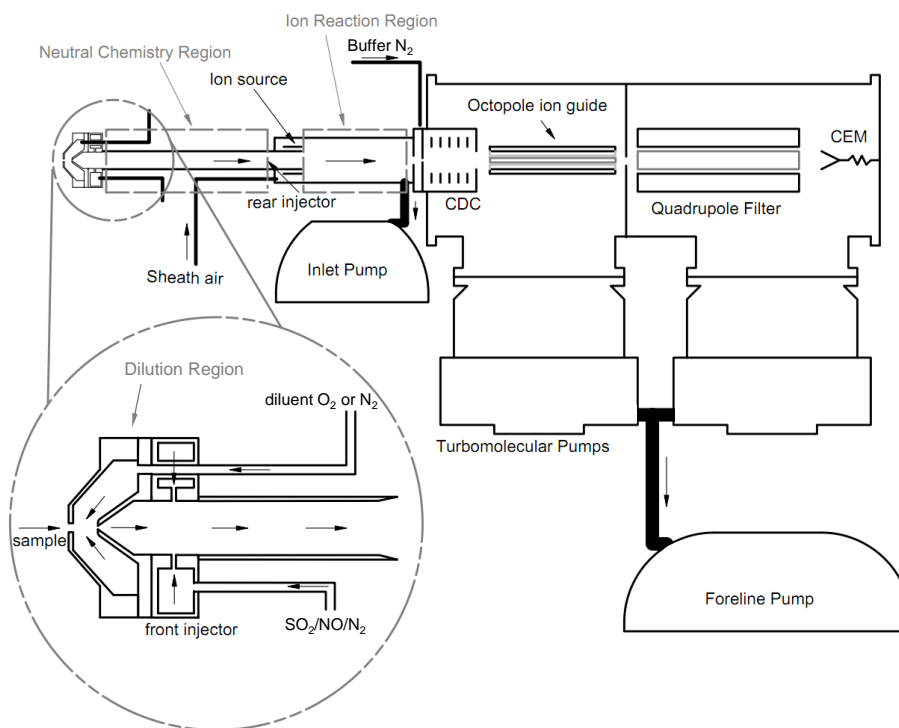
Fig. 1. Schematic of PeRCIMS instrument, with inset of modified inlet and dilution region.

pressures. Diluent gas switching is computer controlled using two low-volume 3-way valves (Clippard) to maintain a constant flow of gas into the dilution region and to minimize pressure pulses in the diluent delivery tubing.

2.3 Inlet conversion chemistry

The mixture of sampled air and diluent is drawn from the dilution region through a 0.50-mm diameter orifice into the neutral chemistry region of the inlet, controlled at a constant pressure of 2.00×10^4 Pa by a scroll pump (Air Squared) and a pressure controller (MKS 640). Two reagent mixtures, 1.5% NO in N$_2$ and 4.0% SO$_2$ in N$_2$ (made in house using pure NO and SO$_2$ gases and UHP N$_2$) are added via the front injector at computer-controlled flow rates to generate NO mixing ratios of 15.0 and 67.5 ppmV and SO$_2$ mixing ratios of 400 and 1800 ppmV for the HO$_2$ + RO$_2$ and HO$_2$ modes, respectively.

In both modes, HO$_2$ radicals are chemically converted via Reactions (R5–R8) into gas phase H$_2$SO$_4$ with a Δ[H$_2$SO$_4$]/[HO$_2$]$_o$ yield of 5.5. As described by Edwards et al. (2003), ambient OH radicals are measured alongside peroxy radicals in the PeRCIMS inlet. However, because ambient [HO$_2$]/[OH] ratios in the troposphere are typically 50–100, the impact of OH on peroxy radical signals is insignificant given that peroxy radical measurement uncertainties are generally ±35%.

The conversion chemistry involved in the measurement of organic peroxy radicals by CIMS was described by Edwards and colleagues as being only slightly more complex than the measurement of HO$_2$, involving an initial conversion of RO$_2$ radicals with available α-hydrogen atoms to HO$_2$ via Reactions (R1) and (R3). With inlet conditions at a reduced pressure and relatively low [NO] such that k_3[O$_2$] > k_2[NO][M], alkoxy radicals formed in Reaction (R1) will form HO$_2$ radicals which are then converted to H$_2$SO$_4$ in the same manner as ambient HO$_2$. From extensive characterization experiments on the modified PeRCIMS inlet using a number of different RO$_2$ precursors at [NO]/[O$_2$] < 1 × 10^{-5}, we have determined that there is an additional reaction pathway by which organic peroxy radicals are converted into H$_2$SO$_4$ in the PeRCIMS inlet. We will explore the inlet chemistry further in the discussion section.

2.4 Background measurement

Ambient H$_2$SO$_4$ and other chemical artifacts that react with SO$_2$ in the inlet to form H$_2$SO$_4$ add to the peroxy radical signal, and thus each peroxy radical measurement in each mode is accompanied by a background measurement. To quantify the background, the SO$_2$ mixture that is added to the front injector during the signal measurement is redirected to the rear injector of the neutral chemistry region (see Fig. 1). The inlet chemistry proceeds such that OH radicals formed in Reaction (R5) react with NO to form HONO

via Reaction (R9) prior to encountering SO_2, preventing the conversion of ambient peroxy radicals into H_2SO_4. The SO_2 mixture is directed to either the front or rear injector by a low-volume computer-controlled 3-way valve (Clippard). To maintain constant and balanced flows through the injectors for the entire measurement cycle for both modes, additional quantities of N_2 gas are added to the front and rear injectors. For typical operation, the duration of the background measurement is equal to the duration of the signal measurement. The actual peroxy radical concentration for each measurement mode is determined using the difference in the signal and background measurements.

2.5 Ion chemistry

Immediately following the neutral chemistry region of the inlet is the ion chemistry region where a fraction of the gas-phase H_2SO_4 molecules is converted into HSO_4^- ions via a proton-transfer reaction with NO_3^- ions and its clusters, similar to the reaction scheme described by Tanner and Eisele (1995):

$$NO_3^- + H_2SO_4 \longrightarrow HNO_3 + HSO_4^-. \tag{R10}$$
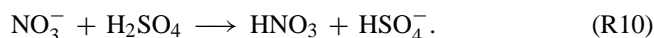
A mixture of air, nitric acid vapor and NO is added to the inlet at the end of the neutral chemistry region to provide a sheath flow within the ion chemistry region. This sheath mixture includes 2.32 SLPM of ambient air that has passed through a chemical scrubber to remove trace SO_2, as well as 1.5 sccm of N_2 that has passed through the headspace of a vial containing liquid concentrated HNO_3 and ≈ 5 sccm of the 1.5% NO in N_2 mixture. NO_3^- ions are produced as the HNO_3 vapor in the sheath flow is ionized by O_2^- and other more primary products generated by the radioactive source (^{241}Am). The NO added to the sheath air helps to lower the background by reacting with OH and other radicals produced by the source emission.

2.6 Ion detection

At the rear of the ion region, HSO_4^- ions are directed through a 0.2-mm diameter pinhole by a series of ion lenses located throughout the inlet and inside the vacuum system, along with other negatively-charged ions (i.e. NO_3^- and clusters of NO_3^- or HSO_4^- with neutral species). An N_2 buffer flow (200 sccm), immediately before the pinhole and greater than the flow into the pinhole, serves to prevent oxygen and other neutral gases from entering the vacuum system, while allowing ions, with the help of an electric field, to pass through while also reducing H_2O clustered with the ions.

For different applications or platforms, the PeRCIMS inlet has been affixed to a number of different vacuum systems including two single-channel systems each housing a single quadrupole and detector, and a 4-channel CIMS system with four inlet mounting locations and four quadrupoles and detectors. The primary components in these vacuum systems

are similar. Depending on the diameter and volume of the vacuum system, two or three turbomolecular pumps (Varian V550, Varian V301, Balzer-Pfeiffer TCP-380), mounted orthogonally to the ion stream and backed by a scroll pump (Air Squared, Synergy or Varian) are used to differentially pump the vacuum system to pressures of 1×10^{-3} Pa or less. Immediately behind the pinhole is a collision dissociation chamber (CDC) which accelerates and aids in the dissociation of ion clusters, leaving primarily NO_3^- and HSO_4^- ions. The CDC region is kept at a constant pressure, ideally 10 Pa, determined by the diameter of the orifice at the rear of the CDC, which is typically between 6 and 10 mm. After passing through the CDC, ions are guided further into the vacuum system either by a series of ion lenses or by an octopole ion guide assembly mounted immediately after the CDC, and are then mass-selected by a quadrupole mass filter with additional ion lenses before and after the quadrupoles. At the rear of the vacuum system, the ions selected by the mass filter are detected by a channel electron multiplier (CEM) (Ceramax, K & M Electronics) biased in the negative ion pulse counting mode.

The ratio of the NO_3^- and HSO_4^- counting frequencies (counts/s) is proportional to the peroxy radical signal S according to:

$$S = \frac{\left(f_{HSO_4^-,\text{signal}}\right) - \left(f_{HSO_4^-,\text{background}}\right)}{\left(f_{NO_3^-}\right) - \left(f_{\text{electronic noise}}\right)} \tag{1}$$

where $f_{HSO_4^-,\text{signal}}$ and $f_{HSO_4^-,\text{background}}$ are the HSO_4^- counting frequencies when the SO_2 mixture is directed through the front and rear injectors, respectively, and $f_{\text{electronic noise}}$ is the counting frequency of a region of the mass spectrum where there are not typically ions present, typically m/z 20 or 70. The count rates of NO_3^- are statistically identical in the signal and background modes. Generally, $f_{\text{electronic noise}} \ll f_{NO_3^-}$, and thus this correction is only minor and the electronic noise measurement serves to confirm that there is not significant electronic noise present in the system.

2.7 Calibration

Calibration of the sensitivity of the instrument to peroxy radicals is accomplished by a quartz calibration cell positioned in front of the inlet (Fig. 2), H_2O molecules are photolyzed by a low pressure Hg lamp (UVP, Jelight or Hamamatsu) with a fused quartz envelope emitting in the UV range (primarily at 184.9 and 253.7 nm) via:

$$H_2O_{(g)} + h\upsilon \ (184.9 \text{ nm}) \longrightarrow OH + H \tag{R11}$$

$$H + O_2 + M \longrightarrow HO_2 + M. \tag{R12}$$
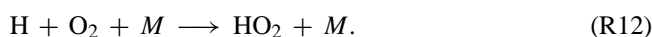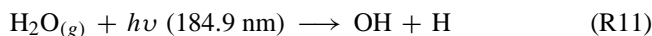
Air at a desired absolute humidity is generated by combining flows of dry synthetic air (United States Welding, Hydrocarbon Free, total hydrocarbons ≤ 0.1 ppmV) with synthetic
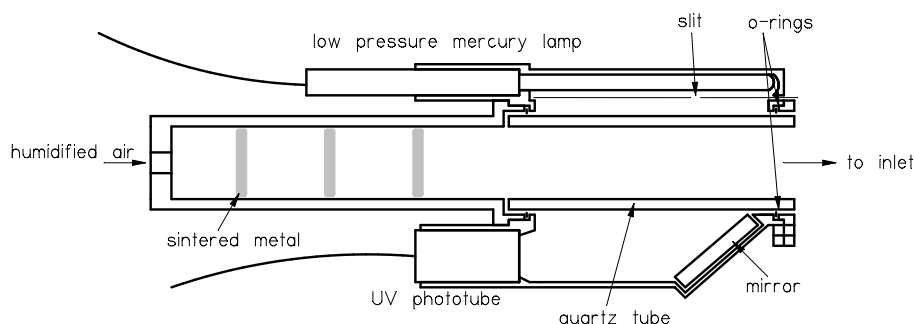
**Fig. 2.** Schematic of new calibration cell.

air that has been saturated by passing through a 303-K temperature-controlled vessel containing PTFE spheres (Hoover Precision Products, Inc.; 1/4-in. diameter) wetted with deionized water. The humidity of the air mixture is monitored continually by directing 100 sccm of the total air mixture flow (5–20 SLPM) through a hygrometer (Dew-Prime III, Edgetech).

Radical production is controlled by varying the amount of radiation passing through the cell and the water vapor mixing ratio of the synthetic air. The amount of radiation in the calibration cell can be controlled by adjusting the distance between the lamp and the cell or by inserting slits of differing widths in the path of the radiation. Both of these properties could be adjusted on the previous calibration cell assembly (shown by Edwards et al., 2003), but only the slit width can be adjusted on the current calibration assembly (Fig. 2). Radical concentrations similar to those found in the atmosphere and greater are generated using this method. From Cantrell et al. (1997a,b), the yield of HO$_2$ radicals from the photolysis of water can be determined using

$$[HO_2] = Y (It) \, \sigma_{H_2O} \, \phi_{H_2O} \, [H_2O], \qquad (2)$$

where σ_{H_2O} is the absorption cross section of water vapor (i.e. 7.22×10^{-20} cm^2 molecule^{-1}) and ϕ_{H_2O} is the photolysis quantum yield (assumed to be unity) at 184.9 nm. Y is a yield factor dependent on the added OH-reactant, equal to 1 for CH$_4$ and other hydrocarbons, and 2 for H$_2$. The quantity It is the product of the lamp flux and the photolysis time, and is determined for each calibration cell assembly in separate N$_2$O actinometry experiments, as described by Edwards et al. (2003), for specific slits and flow rates through the calibration cell.

To generate a fixed hydroperoxy radical concentration, H$_2$ (Matheson or Airgas, >99.99 % purity) is added to the humidified air flow, converting all OH formed in Reaction (R11) to HO$_2$ according to:

$$H_2 + OH \longrightarrow H_2O + H \qquad (R13)$$

$$H + O_2 \, (+M) \longrightarrow HO_2 \, (+M). \qquad (R14)$$
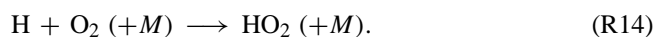
Thus, the total [HO$_2$] produced is $2It\sigma_{H_2O}\phi_{H_2O}$ [H$_2$O]. In the absence of added H$_2$, the OH will react with trace gases in the synthetic air and will create an unknown mixture of hydroperoxy and organic peroxy radicals.

## 3 Instrument characterization

A number of tests have been performed on the PeRCIMS instrument to characterize the inlet chemistry and to establish the ambient measurement modes for optimum sensitivity and separation of HO$_2$ and HO$_2$ + RO$_2$. These characterizations were made using both the previous and current calibration cell assemblies described above for absolute calibrations. In general, H$_2$ or CH$_4$ (or another RO$_2$ precursor) is added to the humidified air that passes through the calibration cell, with the output of the cell directly in front of the PeRCIMS inlet. Generating organic peroxy radicals using H$_2$O photolysis is preferential to using Cl atom + precursor reactions (as in Edwards et al., 2003) as OH chemistry produces RO$_2$ species more commonly encountered in the atmosphere. As with the absolute calibration, OH radicals formed via Reaction (R11) react with H$_2$ to generate a second HO$_2$ for each water molecule photolyzed, according to Reactions (R13) and (R14). Adding CH$_4$ in place of H$_2$ generates a methyl peroxy radical according to:

$$CH_4 + OH \longrightarrow H_2O + CH_3 \qquad (R15)$$

$$CH_3 + O_2 \, (+M) \longrightarrow CH_3O_2 \, (+M), \qquad (R16)$$
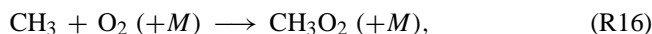
which results in equal parts HO$_2$ and CH$_3$O$_2$ radicals. The background-corrected signals (as in Eq. 1) of the peroxy radicals generated from the addition of the two precursors, S_{CH_4} and S_{H_2}, under otherwise identical inlet conditions, are used to determine $\alpha_{CH_3O_2}$ (the conversion efficiency or measurement sensitivity to CH$_3$O$_2$ in comparison to HO$_2$ which is a function of [NO]/[O$_2$]) or, in general, α_{RO_2} for any organic peroxy radical precursor RH, according to:

$$\alpha_{RO_2} = 2 \times \left(\frac{S_{RH}}{S_{H_2}} \right) - 1. \qquad (3)$$
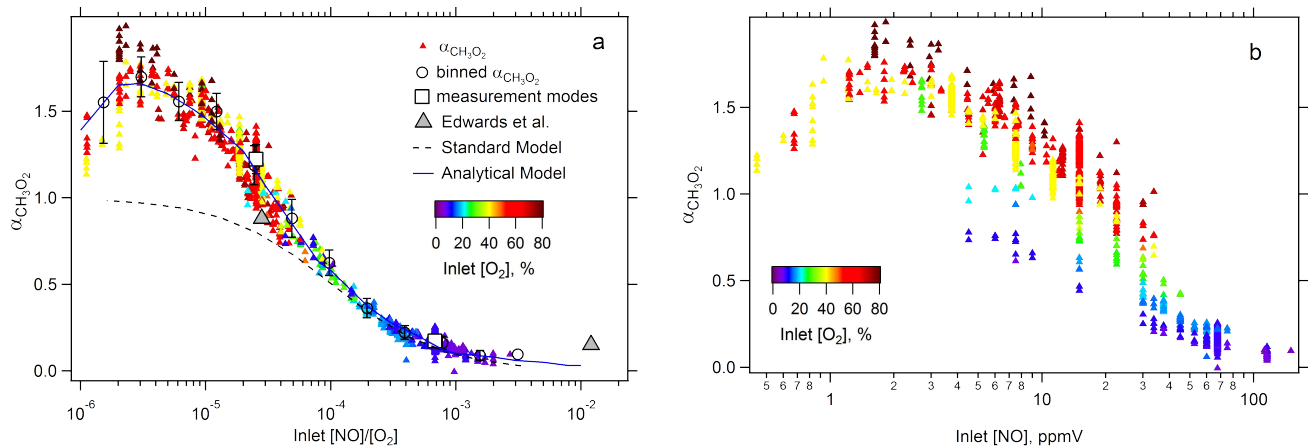
Fig. 3. Plot of measured $\alpha_{CH_3O_2}$ against **(a)** the ratio of [NO]/[O$_2$] in the inlet and **(b)** inlet [NO]. Individual measurements are shown as small triangles, colored according to inlet O$_2$ concentration. In **(a)** the open black circles are the average measured $\alpha_{CH_3O_2}$ values binned by [NO]/[O$_2$], with error bars showing the standard deviation for each bin. Squares are the mean $\alpha_{CH_3O_2}$ values for the two ambient measurement modes. Large grey triangles are the literature $\alpha_{CH_3O_2}$ values reported by Edwards et al. (2003). Also shown are the standard model (dashed curve) and the analytical model (solid blue curve) fit to the results.

Determinations of α_{RO_2} have been made for a number of RO$_2$ precursors over a wide range of [NO]/[O$_2$] values between 10^{-2} and 10^{-6}. Each α_{RO_2} determination requires a peroxy radical measurement with H$_2$ added to the humidified synthetic air, and a peroxy radical measurement with CH$_4$ or another RO$_2$ precursor added. Reported α_{RO_2} values were determined using the means of approximately four consecutive individual S_{RH} and S_{H_2} measurements, such that all measurements are made within approximately 10 min.

To characterize the inlet chemistry and establish the two ambient observation modes, a broad set of operating conditions have been tested with a variety of peroxy radical precursors and concentrations and are described in the following sections. To ensure ideal conditions for each α_{RO_2} determination, individual calibration parameters were investigated to determine ideal operating ranges for the total flow rate through the calibration cell and the concentrations of the radical precursors. The results of these tests are discussed in the following section. Using conditions that fell within these ideal operating parameters, α_{RO_2} has been measured more than 1000 times over a broad range of inlet [NO] and [NO]/[O$_2$]. The results of these measurements are shown in Fig. 3. With inlet [NO] < 2 ppmV, there is less $\alpha_{CH_3O_2}$ dependence on inlet [O$_2$], but for inlet [NO] > 2 ppmV, the concentration of O$_2$ in the inlet plays a more important role in determining $\alpha_{CH_3O_2}$, and the ratio of [NO]/[O$_2$] is key. The $\alpha_{CH_3O_2}$ data were binned by [NO]/[O$_2$] value, and the mean $\alpha_{CH_3O_2}$ values for each bin are shown in Fig. 3a and listed in Table 2 along with the mean $\alpha_{CH_sO_2}$ values for the two ambient measurement modes.

Table 2. Summary of the mean $\alpha_{CH_3O_2}$ values from methane experiments according to inlet [NO]/[O$_2$].

Inlet [NO]/[O$_2$] Range	Mean $\alpha_{CH_3O_2}^{a}$	Number of Measurements[b]
$(2.21$–$4.42) \times 10^{-3}$	0.09	1
$(1.10$–$2.21) \times 10^{-3}$	0.09 ± 0.03	22
$(0.55$–$1.10) \times 10^{-3}$	0.16 ± 0.04	230
$(2.76$–$5.52) \times 10^{-4}$	0.22 ± 0.04	70
$(1.38$–$2.76) \times 10^{-4}$	0.36 ± 0.06	51
$(0.69$–$1.38) \times 10^{-4}$	0.62 ± 0.07	31
$(3.45$–$6.91) \times 10^{-5}$	0.88 ± 0.11	64
$(1.73$–$3.45) \times 10^{-5}$	1.19 ± 0.11	370
$(0.86$–$1.73) \times 10^{-5}$	1.50 ± 0.10	157
$(4.32$–$8.63) \times 10^{-6}$	1.56 ± 0.11	40
$(2.16$–$4.32) \times 10^{-6}$	1.70 ± 0.12	44
$(1.08$–$2.16) \times 10^{-6}$	1.55 ± 0.24	40

Ambient Mode	[NO]/[O$_2$]		
HO$_2$	6.80×10^{-4}	0.17 ± 0.04	159
HO$_2$ + RO$_2$	2.53×10^{-5}	1.22 ± 0.08	159

[a] For [NO]/[O$_2$] ranges in which more than one $\alpha_{CH_3O_2}$ measurement was made, the uncertainty is the standard error of the mean.

[b] Each $\alpha_{CH_3O_2}$ measurement is determined from the mean of four individual peroxy radical measurements with CH$_4$ added to the humidified air and the mean of four measurements with H$_2$ added to the humidified air.

3.1 Calibration parameter experiments

3.1.1 Total flow rate through the calibration cell

The concentration of radicals formed in the calibration cell depends on both the total flow rate of the humidified air mixture through the cell and the amount of irradiation with which
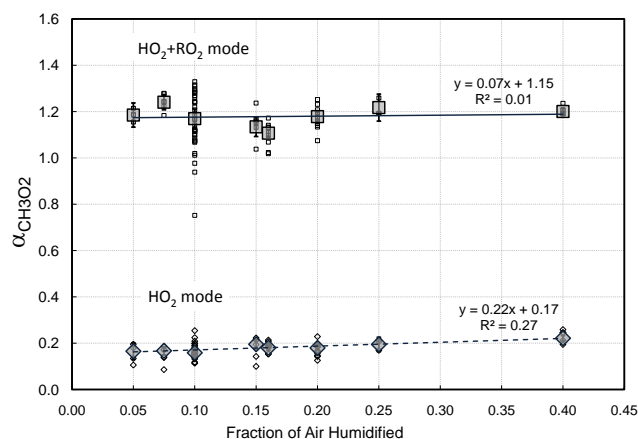
Table 3. Summary of dependence on the total flow of humidified air through the calibration cell.

Dry Air, SLPM	Humidified Air, SLPM	Hg Lamp Distance, inches	Slit Width, inches	HO₂ radicals, pptV	Mean $\alpha^*_{CH_3O_2}$
1.25	0.125	1.0	0.5	210	2.06 ± 0.02
1.25	0.125	2.0	0.5	139	1.81 ± 0.04
1.25	0.125	4.0	0.5	53	1.69 ± 0.02
1.75	0.175	1.0	0.5	234	1.65 ± 0.02
1.75	0.175	2.0	0.5	111	1.39 ± 0.05
1.75	0.175	4.0	0.5	49	1.36 ± 0.03
2.50	0.250	1.0	0.5	221	1.30 ± 0.02
2.50	0.250	2.0	0.5	123	1.22 ± 0.03
2.50	0.250	4.0	0.5	40	1.21 ± 0.02
3.75	0.375	1.0	0.5	172	1.19 ± 0.02
3.75	0.375	2.0	0.5	90	1.12 ± 0.02
3.75	0.375	4.0	0.5	29	1.10 ± 0.03
5.00	0.500	1.0	0.5	137	1.10 ± 0.03
5.00	0.500	2.0	0.5	68	1.08 ± 0.03
5.00	0.500	4.0	0.5	23	1.14 ± 0.02

* Uncertainties are the standard errors of the mean $\alpha_{CH_3O_2}$ values.

Fig. 4. Dependence of $\alpha_{CH_3O_2}$ on the fraction of calibrator air that has been saturated for the HO₂ + RO₂ and HO₂ modes. Smaller points show individual $\alpha_{CH_3O_2}$ measurements, and larger points are the error-weighted means of the $\alpha_{CH_3O_2}$ determinations at each humidity. Error bars show the error-weighted standard errors.

the water vapor in the air is exposed, It (Eq. 3). The ideal total flow rate through the calibration cell was determined for three lamp intensities (generated with the lamp at three different distances from the cell using the old calibration cell apparatus) at five different total calibration cell flow rates. For each flow rate, the relative flow rates of saturated and dry air were held constant at 1:10, or approximately 9.1% relative humidity at room temperature. For all measurements reported for this test the inlet $[NO]/[O_2]$ was 1.29×10^{-5} with 1.0 SLPM of O_2 added to the dilution region, and 10 sccm each CH_4 and H_2. A minimum of two $\alpha_{CH_3O_2}$ measurements (8 individual measurements with each precursor) were made for each lamp distance at each total air flow rate. A summary of the results of the test is shown in Table 3.

The measured $\alpha_{CH_3O_2}$ values indicate that with a specified concentration of water, a minimum flow rate through the calibration cell is necessary, as it is otherwise possible to generate too many peroxy radicals to be quantitatively converted to H_2SO_4 without requiring a correction for NO_3^- depletion in the inlet. Also, wall loss of radicals becomes more important at slow flow rates. This can impact $\alpha_{CH_3O_2}$ determinations because HO₂ is lost more readily on surface contact than CH_3O_2. Tests with similar It from different calibrator configurations showed that with flow rates through the calibrator of 3 SLPM or greater, wall loss is not significant. With a constant water vapor mixing ratio, a smaller total flow rate results in a longer exposure time to irradiation in the calibration cell and thus a larger fixed radical concentration. To avoid needing to correct for NO_3^- depletion, calibrations made at a minimum flow rate of $\approx$3 SLPM of synthetic air at a relative humidity of $\approx$10% at room temperature through the calibration cell is ideal. A standard operating procedure using 5 SLPM of 10% humidified air has been adopted based on these results.
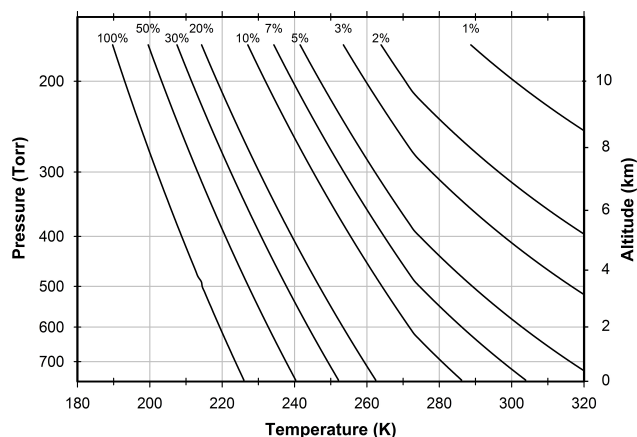
3.1.2 Water vapor mixing ratio

The modified PeRCIMS inlet has also been tested using a range of water vapor mixing ratios in the calibration cell air mixture to establish whether there is stability in $\alpha_{CH_3O_2}$ at the ambient mode conditions across a range of humidities. The total flow through the calibration cell was held constant at 5 SLPM, but the relative flows of saturated air and dry synthetic air were adjusted to generate humidified fractions ranging from 5 to 40% of the total flow. During these measurements, alternating diluent N_2 and O_2 were added to generate a 1:1 ratio with the sample air from the calibration cell, and 10 sccm of alternating CH_4 and H_2 were added to the humidified air. The resulting $\alpha_{CH_3O_2}$ values, as well as the error-weighted mean $\alpha_{CH_3O_2}$ value for each humidity studied are shown in Fig. 4.

From the water vapor calibration test, $\alpha_{CH_3O_2}$ appears to be independent of the humidity of the calibration air mixture over a range of saturations from 5 to 25%. Based on the results from this test, we have confidence in other experiments that were performed under similar conditions with 10% saturated air in the calibration cell. There is, however, a lower limit on the absolute water vapor mixing ratio in the inlet for conversion of ambient peroxy radicals into H_2SO_4. This is based on Reaction (R8), in which the rate of the conversion of SO_3 into H_2SO_4 is proportional to the square of the water mixing ratio in the inlet. We have calculated the lower limit for water content over a range of atmospheric relative humidities and temperatures, and have determined that the PeRCIMS is sufficiently sensitive (i.e. the calibration factors are stable with regards to the measurement of peroxy radicals) under the majority of tropospheric conditions. However, because the sampled air is drawn from ambient pressure into a low pressure region and being diluted
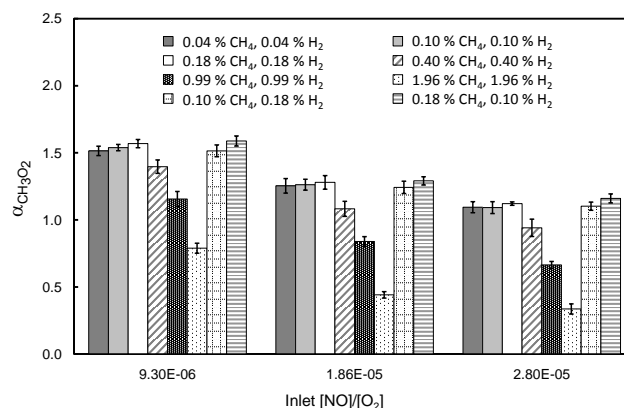
Fig. 6. Dependence of $\alpha_{CH_3O_2}$ on the H$_2$ and CH$_4$ mixing ratios in the calibration cell air mixture at three inlet [NO]/[O$_2$] conditions. Error bars show the standard error of each $\alpha_{CH_3O_2}$ determination.

1:1 with dry N$_2$ or O$_2$, there are possible ambient conditions in which the measurement sensitivity could be lowered. This typically involves air masses that are very dry and cold, i.e. measurements at low altitudes in dry arctic regions. Figure 5 shows the calculated dependence on ambient pressure and temperature for a series of minimum relative humidities at which peroxy radicals can be measured without any modifications to the sampling procedure. For field studies in which conditions are below these minimum relative humidity curves, we have developed a method in which a fraction of the diluents (N$_2$ and O$_2$) are humidified to add sufficient water vapor to the inlet. In these situations, the exact amount of water vapor in the inlet is not important as long as it is above the critical lower limit value.

3.1.3 Peroxy radial precursor concentration

The calibration and α_{RO_2} characterizations of the peroxy radical measurement rely on the OH-chemistry of CH$_4$ and H$_2$ in the calibration cell to generate reproducible mixing ratios of HO$_2$ and CH$_3O_2$. When insufficient amounts of CH$_4$ or H$_2$ are added to the humidified air, trace contaminants in the air or other reagent gases can react with OH in place of CH$_4$ and H$_2$, generating unknown [CH$_3O_2$], [HO$_2$] or other radicals. With excessively high CH$_4$ or H$_2$ mixing ratios, the conversion of CH$_3O_2$ and HO$_2$ to H$_2$SO$_4$ in the inlet will not reach completion due to competition with SO$_2$ for OH. To determine the ideal concentration range of peroxy radical precursors in the calibration cell flow, two tests were performed using a range of CH$_4$ and H$_2$ flow rates added to the total calibration flow.

In the first test, $\alpha_{CH_3O_2}$ was determined at three [NO]/[O$_2$] ratios (9.30×10^{-6}, 1.86×10^{-5}, 2.80×10^{-5}) for a series of CH$_4$ mixing ratios (0.04, 0.10, 0.18, 0.40, 0.99, and 1.96,

all % by volume) in 5.0 SLPM of 10% humidified air. For the first six tests [H$_2$] was kept equal to [CH$_4$] for each $\alpha_{CH_3O_2}$ determination, and for the last two tests, [H$_2$] was approximately twice and half the CH$_4$ mixing ratios of 0.10% and 0.18%, respectively. For each CH$_4$ mixing ratio, $\alpha_{CH_3O_2}$ is reported as the average of at least four determinations made at each inlet [NO]/[O$_2$], generated by diluting the air from the calibration assembly by one quarter with O$_2$ and adding NO to the front injector to generate inlet NO mixing ratios of 3.75, 7.50 and 11.25 ppmV, respectively. The results of this experiment are shown in Fig. 6.

From the first precursor test, the resultant hydroperoxy radical signal from the addition of H$_2$ did not vary outside the measurement uncertainty with H$_2$ concentrations ranging from 0.010% to 0.99%. Thus, the measured $\alpha_{CH_3O_2}$ is significantly less sensitive to the absolute H$_2$ concentration in the calibration mixture than it is to the concentration of the RO$_2$ precursor. For this reason, [H$_2$] was held constant during the second precursor concentration test at a concentration large enough to ensure that the HO$_2$ radicals measured were formed from the photolysis of water and the reaction of OH with H$_2$.

The second test involved a series of $\alpha_{CH_3O_2}$ determinations in the two ambient modes, with [NO]/[O$_2$] ratios of 2.80×10^{-5} and 6.80×10^{-4}. For this test, a wider range of [CH$_4$] in the air mixture was generated using single and double dilution techniques to add CH$_4$ to a 5.0 SLPM flow of humidified air. For the single-dilution technique, between 2 and 100 sccm of CH$_4$ was added directly to the humidified air via a 100 sccm mass flow controller (MFC). The double dilution required an initial step in which a small flow of CH$_4$ was added to a secondary flow of synthetic air using a 10 sccm MFC and the resulting diluted mixture of CH$_4$ in air was added to the humidified air via the 100 sccm MFC. During the double dilution, the initial CH$_4$ in air mixture was vented to maintain a constant pressure $\approx 2.5 \times 10^3$ Pa above ambient

Table 4. Dependence of calibration factors and $\alpha_{CH_3O_2}$ values on calibration cell pressure.

Calibration	F, $\times 10^3$		$\alpha^*_{CH_3O_2}$	
Cell Pressure, $\times 10^4$ Pa	HO$_2$ + RO$_2$ mode	HO$_2$ mode	HO$_2$ + RO$_2$ mode	HO$_2$ mode
9.33	18.2 ± 1.0	14.8 ± 1.0	1.26 ± 0.05 (12)	0.15 ± 0.02 (12)
8.40	18.3 ± 1.0	14.5 ± 1.0	1.20 ± 0.08 (17)	0.16 ± 0.04 (17)
6.67	17.6 ± 1.0	15.9 ± 1.0	1.24 ± 0.05 (4)	0.17 ± 0.03 (4)
5.33	16.8 ± 1.3	17.6 ± 1.0	1.20 ± 0.08 (21)	0.15 ± 0.04 (21)
4.00	17.7 ± 1.9	16.8 ± 2.2	1.16 ± 0.07 (4)	0.17 ± 0.02 (4)

^{a} Mean $\alpha_{CH_3O_2}$ values are shown, with the number of individual determinations used in the mean in parentheses. Errors are the standard errors of the means.

pressure, allowing a constant flow through the 100 sccm MFC. Using the two dilution techniques, calibration-cell methane concentrations ranging from 20 ppmV to 2.0% were generated for subsequent $\alpha_{CH_3O_2}$ measurements. For this experiment, [H$_2$] in the calibration flow was kept constant at 0.18% for the $\alpha_{CH_3O_2}$ determinations. The results of this experiment are shown in Fig. 7.

From the second precursor test, it is evident that there are both upper and lower limits for the required concentration of RO$_2$ precursors in the calibration cell. With decreasing CH$_4$ concentrations of 0.010% or less, the measured $\alpha_{CH_3O_2,low}$ values for the HO$_2$ + RO$_2$ mode decrease significantly, most likely due to trace species in the synthetic air reacting with OH in place of CH$_4$. With increasing calibration-cell methane concentrations of 1.0% or greater, the measured $\alpha_{CH_3O_2}$ values for both measurement modes decrease significantly. In this case, the decrease in $\alpha_{CH_3O_2}$ is likely due to the incomplete chemical conversion of peroxy radicals into H$_2$SO$_4$. Thus, for ongoing calibration purposes, the concentration of RO$_2$ precursors in the calibration cell should fall between 0.010% and 1.0% equivalent methane reactivity, ideally in the range of 0.05% to 0.2%, corresponding to an OH reactivity between 60 and 250 s^{-1}.

Using the optimized conditions established for the above calibration cell parameters, i.e. total flow rate through the calibration cell, water vapor concentration in the calibration cell air mixture, and RO$_2$ precursor concentration, the parameters described in the following sections were explored to better characterize the PeRCIMS instrument.

3.2 PeRCIMS characterization experiments

3.2.1 Ambient pressure dependence

A modified calibration cell that can be sealed onto the sample intake end of the PeRCIMS inlet was used to determine the dependence of $\alpha_{CH_3O_2}$ on ambient pressure. For this test, absolute calibrations and $\alpha_{CH_3O_2}$ determinations were made in the HO$_2$ and HO$_2$ + RO$_2$ measurement modes at a range of calibration cell pressures. To achieve a range of pressures
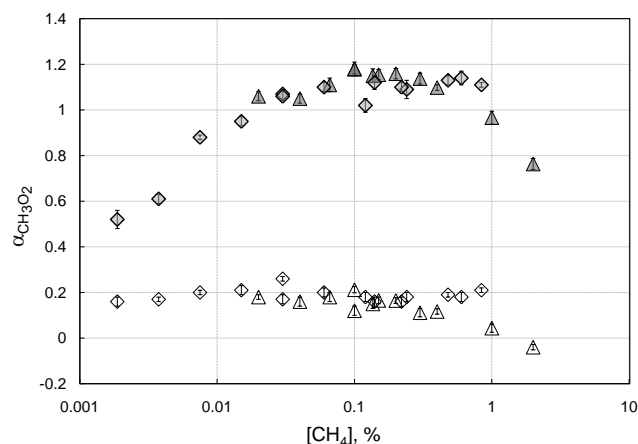
Fig. 7. Dependence of $\alpha_{CH_3O_2}$ on CH$_4$ mixing ratio in the calibration cell. Closed and open symbols are the measured $\alpha_{CH_3O_2}$ values at the HO$_2$ + RO$_2$ mode and HO$_2$ mode, respectively, and triangles and diamonds are the results from the single-dilution and double-dilution measurements, respectively. Error bars show the standard errors of each $\alpha_{CH_3O_2}$ determination.

at the PeRCIMS intake, a pressure controller and pump were attached to a side port on the calibration cell, downstream of the Hg lamp, to control the pressure in the calibration cell to a desired pressure between 4.00×10^4 and 9.33×10^4 Pa. For these measurements, the air mixture in the cell consisted of 5 SLPM of 10% saturated synthetic air with alternating CH$_4$ and H$_2$ at 0.18%, and the flow rates of the reagent gases and diluents were adjusted according to the sample flow rate into the inlet from the calibration cell. The results from this test are listed in Table 4. Fitted slopes of the results for $\alpha_{CH_3O_2}$ versus pressure for the HO$_2$ and HO$_2$ + RO$_2$ modes are statistically insignificant at the 98% Confidence Interval. This is consistent with the inlet being at a constant reduced pressure, and thus the inlet chemistry regulating the conversion of peroxy radicals into H$_2$SO$_4$ is independent of the pressure outside the inlet.

The primary concern with regards to ambient pressure is for high-altitude measurements as the sample flow into the inlet is affected. The flow of gas into the inlet is proportional to the ambient pressure (P_{amb}) provided $\Delta P / P_{amb} > 0.5$, where ΔP is the difference between ambient P and the inlet P (Green and Perry, 2007). When $\Delta P / P_{amb}$ is less than 0.5, the flow is a function of both the ambient and inlet P. Thus, for ambient pressures less than 4.00×10^4 Pa, the flow through the orifice into a 2.00×10^4 Pa inlet becomes a non-linear function of P_{amb}. Although the inlet chemistry has been optimized for an inlet pressure of 2.00×10^4 Pa, we are developing a method for high-altitude measurements, where $P_{amb} < 4.00 \times 10^4$ Pa, such that the computer-controlled inlet pressure is reduced to maintain a sufficient sample flow.

3.2.2 RO$_2$ precursor characterization

The sensitivity dependencies of the PeRCIMS instrument to CH$_3$O$_2$ radicals on the ratio of [NO]/[O$_2$] and on the absolute concentration of [NO] in the inlet have been shown (Fig. 3). However, the general term RO$_2$ includes many other organic peroxy radical species which may undergo different chemistry in the PeRCIMS inlet. Thus, the sensitivity of the PeRCIMS measurement to organic peroxy radicals other than CH$_3$O$_2$ must be quantified.

Edwards et al. (2003) reported a series of α_{RO_2} values for organic peroxy radicals generated via reactions of Cl atoms with a series of RO$_2$ precursors including alkanes, alkenes and aromatic compounds. These α_{RO_2} were determined at two inlet [NO]: essentially an HO$_2$ mode and an HO$_2$ + RO$_2$ mode with inlet [NO]/[O$_2$] ratios of approximately 1.2×10^{-2} and 2.8×10^{-5}, respectively. In ambient air, however, the majority of RO$_2$ radicals are formed via OH-oxidation of the parent hydrocarbon. Hence, the α_{RO_2} values that we report here are based on measurements of RO$_2$ generated from reactions with OH radicals. This is of particular importance for peroxy radicals from OH-reactions with unsaturated non-methane hydrocarbons (NMHC), which typically differ from those generated via unsaturated NMHC-Cl reactions (Orlando et al., 2003; Suh et al., 2003; Taatjes, 1999; Atkinson, 2000). As well, we present measurements of α_{RO_2} for a number of RO$_2$ precursors at not just two ambient measurement modes, but over a range of inlet [NO] and [O$_2$].

The same double dilution apparatus discussed in the previous section for adding small flows of methane to the calibration flow was employed here. Gas-phase RO$_2$ precursors were added via the 10-sccm mass flow controller such that the combined flow rates from the two dilutions resulted in OH reactivities within the optimized range for methane reactivity (60 to 250 s^{-1}). For RO$_2$ precursors in the liquid phase at room temperature, dry synthetic air was passed through the 10-sccm mass flow controller, then through the headspace of a vial containing a small volume of the precursor. The pressure in the vial and manifold was monitored and vented

through a needle valve to maintain a constant pressure approximately 2.5×10^3 Pa above ambient. Thus, the concentration of the precursor in the synthetic air flow could be calculated from its vapor pressure, and an appropriate amount was added to the calibration gas flow to generate OH reactivities in the ideal range.

A total of 17 different NMHC RO$_2$ precursors were used to create RO$_2$ radicals that were subsequently measured using the PeRCIMS instrument across a range of [NO]/[O$_2$]. The results of the α_{RO_2} determinations for each of these precursors were grouped into three different subgroups, C$_2$-C$_5$ alkanes (i.e. NMHC with between two and five carbon atoms), C$_6$-C$_7$ alkanes, and unsaturated hydrocarbons. These are plotted along with the measurements of α_{RO_2} for comparison in Fig. 8. For some RO$_2$ precursors, a mixture of RO$_2$ radicals are generated during reaction with OH and the reported α_{RO_2} values are a weighted mean of the individual values. For each precursor, the mean of the α_{RO_2} determinations made within ±15% of the two ambient measurement modes are listed in Table 5 with literature OH rate coefficients.

In Fig. 8a, it is clear that the majority of C$_2$-C$_5$ alkane precursors generate RO$_2$ radicals with similar α_{RO_2} behavior to methylperoxy radicals, but with slightly higher RO$_2$ sensitivity over the entire [NO]/[O$_2$] range measured. Overall, the separation between the HO$_2$-mode and HO$_2$ + RO$_2$-mode ($\Delta\alpha_{RO_2}$) is similar to methane for each of these RO$_2$ precursors. The primary exceptions to this are methylpropane with significantly lower α_{RO_2} values over the entire range of [NO]/[O$_2$] measured, and *n*-pentane with α_{RO_2} values that deviate from those of the other precursors such that they are much higher than $\alpha_{CH_3O_2}$ in the HO$_2$ mode region. Possible reasons for these differences are discussed below.

The majority (>70% at or below 298 K) of methylpropane-OH reactions occur via abstraction of the tertiary hydrogen, resulting in a *tert*-butoxy radical after subsequent reaction with NO (Eq. 1) in the PeRCIMS inlet (Atkinson, 1997; Tully et al., 1986). With no α-hydrogen atoms, the *tert*-butoxy radical cannot react with O$_2$ to generate HO$_2$ via Reaction (R3). Rather, it either decomposes unimolecularly to generate a methyl fragment which must undergo further reaction in the inlet to generate HO$_2$ (decomposition lifetime is ≈1.3 ms at 298 K and 2.00×10^4 Pa and is in the fall-off region) (Blitz et al., 1999; Atkinson, 2007) or react with NO via Reaction (R2) to form *tert*-butylnitrite ($k_{NO, 295 K} = (2.9 \pm 0.2) \times 10^{-11}$ cm^3 s^{-1}, 9.3×10^3 to 8.0×10^4 Pa (Lotz and Zellner, 2000; Atkinson, 2007). With 15 ppmV [NO] in the 2.00×10^4 Pa inlet, the rate of *tert*-butoxy + NO is ≈0.5 ms, and 0.1 ms with 67.5 ppmV [NO], hence the sensitivity of the PeRCIMS instrument to *tert*-butylperoxy radicals is low. The signal that is seen from the methylpropane reaction is due to the OH-abstraction of a primary hydrogen atom, resulting in 2-methylpropoxy radicals. The results for 3-methylpentane in Fig. 8b indicate similar behavior, with α_{RO_2} values that tend
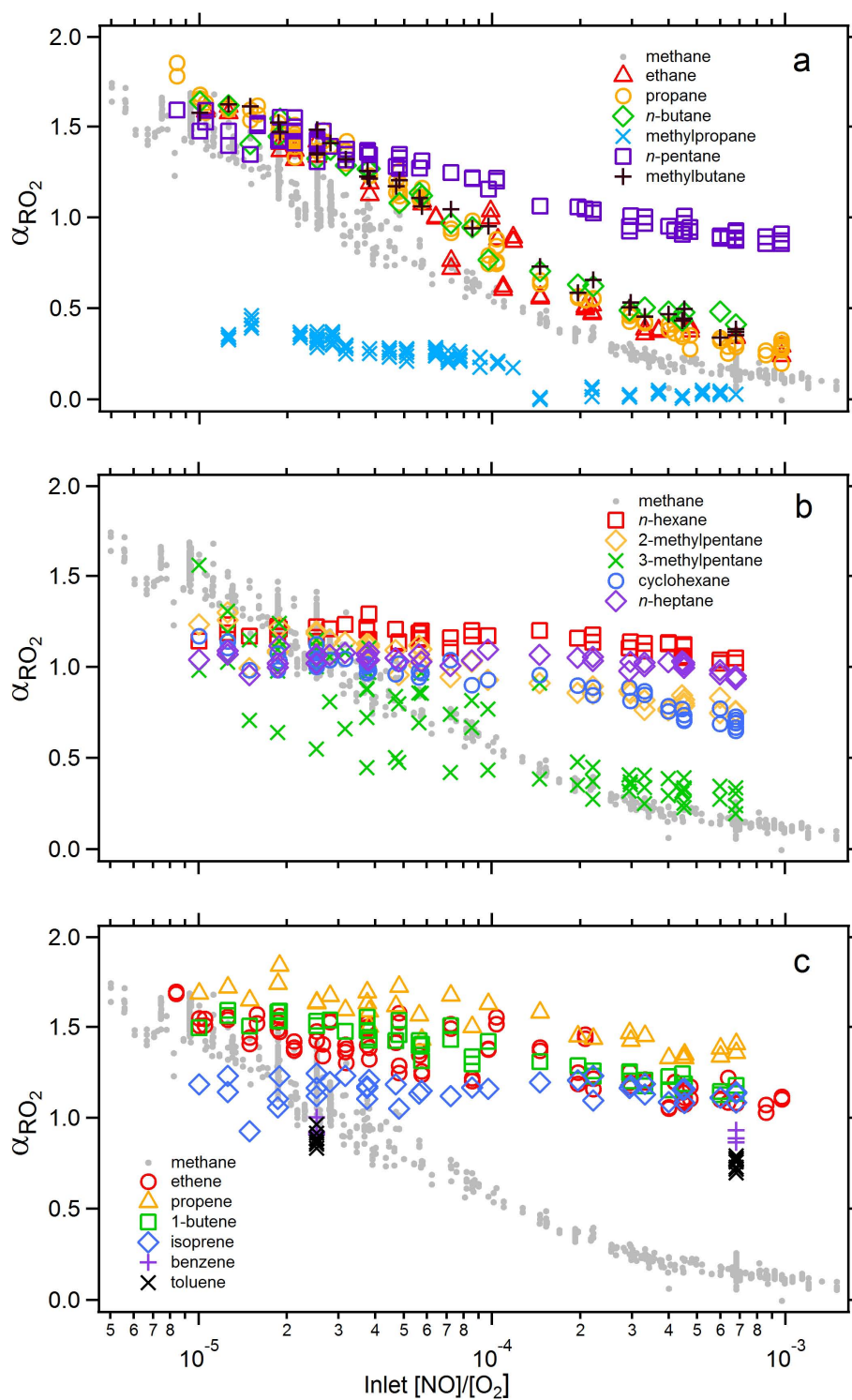
Fig. 8. Plots of α_{RO_2} for RO$_2$ formed from **(a)** C$_2$-C$_5$ (i.e. having between two and five carbon atoms) alkane precursors **(b)** C$_6$-C$_7$ alkane precursors and **(c)** unsaturated hydrocarbon precursors against the ratio of [NO]/[O$_2$] in the inlet. For comparison, measured $\alpha_{CH_3O_2}$ values are included on each plot.

Table 5. Summary of mean α_{RO_2} values from studied RO$_2$ precursors.

RO$_2$ Precursor	$10^{-12} \times k_{OH}^{a}$ (298 K) (cm^3 molecule^{-1} s^{-1})	Mean $\alpha_{RO_2}^{b}$	
		HO$_2$ + RO$_2$ mode	HO$_2$ mode
methane	0.00640	1.22 ± 0.08 (159)	0.17 ± 0.04 (159)
ethane	0.248	1.38 ± 0.06 (2)	0.342 ± 0.003 (2)
propane	1.09	1.41 ± 0.04 (6)	0.30 ± 0.03 (6)
n-butane	2.36	1.35 ± 0.03 (2)	0.45 ± 0.05 (2)
methylpropane	2.12	0.33 ± 0.03 (27)	0.03 ± 0.01 (4)
n-pentane	3.80	1.41 ± 0.05 (8)	0.89 ± 0.02 (9)
methylbutane	3.6	1.40 ± 0.06 (4)	0.36 ± 0.02 (4)
n-hexane	5.20	1.20 ± 0.03 (3)	1.03 ± 0.01 (4)
2-methylpentane	5.2	1.18 ± 0.02 (3)	0.77 ± 0.04 (4)
3-methylpentane	5.2	0.94 ± 0.23 (6)	0.28 ± 0.06 (6)
cyclohexane	6.97	1.04 ± 0.04 (7)	0.70 ± 0.04 (8)
n-heptane	6.76	1.05 ± 0.02 (4)	0.95 ± 0.02 (5)
ethene	8.52	1.45 ± 0.07 (7)	1.11 ± 0.05 (7)
propene	26.3	1.65 ± 0.02 (3)	1.37 ± 0.03 (4)
1-butene	31.4	1.52 ± 0.02 (3)	1.15 ± 0.02 (4)
isoprene	100	1.18 ± 0.05 (4)	1.12 ± 0.03 (4)
benzene	1.22	0.94 ± 0.05 (3)	0.89 ± 0.03 (3)
toluene	5.63	0.89 ± 0.04 (8)	0.75 ± 0.03 (8)

[a] From Atkinson and Arey (2003).

[b] Uncertainties are the standard errors in the mean α_{RO_2} for values measured at inlet [NO]/[O$_2$] ratios within ±15% of the HO$_2$ and HO$_2$ + RO$_2$ modes (see Table 1). Numbers in parentheses are the numbers of individual values used to determine the means.

to be lower than other C$_6$ alkanes. This is consistent with the formation of alkoxy radicals with no α-hydrogen atoms. However, this behavior is not evident in the methylbutane and 2-methylpentane results (Fig. 8a and b), both having α_{RO_2} values closer to the n-alkane with the same number of straight-chain carbon atoms.

From the n-pentane precursor reactions, the measured α_{RO_2} values are increasingly larger than $\alpha_{CH_3O_2}$ values with increasing [NO]/[O$_2$], as are the α_{RO_2} values from the C$_6$ and C$_7$ alkane precursors in Fig. 8b. This is most likely due to n-pentane and larger alkanes having sufficient numbers of carbon atoms to generate alkoxy radicals that are subject to isomerization. These isomerizations often result in reactions that generate HO$_2$ radicals, lowering the separation dependence on the [NO]/[O$_2$] ratio. Figure 8a and b show that as the numbers of carbon atoms in alkanes increase, the ability to deselect the resultant RO$_2$ radical in the HO$_2$ mode decreases, and thus the separation between HO$_2$ and HO$_2$ + RO$_2$ becomes smaller.

In Fig. 8c, the α_{RO_2} values from the unsaturated NMHC precursors have a similar dependence on [NO]/[O$_2$] as larger alkane RO$_2$ precursors. In general, alkene-OH reactions occur as addition reactions, forming hydroxyalkyl radicals that react with O$_2$ under atmospheric conditions to form β-hydroxyalkyl peroxy radicals (and δ-hydroxyalkyl peroxy radicals where conjugated double bonds are present). In high [NO] environments (i.e. the PeRCIMS inlet), these

peroxy radicals react with NO forming primarily hydroxyalkoxy radicals that can decompose unimolecularly (typically generating HO$_2$), isomerize or react with O$_2$ to carbonyl compounds and HO$_2$ (Atkinson, 1997). Thus, in the PeRCIMS inlet, Reaction (R2) is unsuitable for suppression of the conversion of the hydroxyalkoxy radical to HO$_2$ for alkene-precursor RO$_2$ and therefore the separation between HO$_2$ and HO$_2$ + RO$_2$ is lessened. Aromatic hydrocarbons undergo a combination of addition and abstraction reactions with OH radicals (Atkinson, 2000), so with benzene and toluene as RO$_2$ precursors, the impact of rearrangement and dissociation leading to HO$_2$ is seen in the observed α_{RO_2}, but to a lesser degree. Overall, due to the differences in sensitivity of the PeRCIMS to different RO$_2$ radicals, the uncertainties of reported measurements of ambient HO$_2$ account for the relative reactivity of RO$_2$ precursors in the air masses being studied, e.g.: in urban regions with elevated relative reactivity of unsaturated NMHC RO$_2$ precursors, reported HO$_2$ uncertainties must account for RO$_2$ that may be observed in the HO$_2$ mode. This is addressed in Sect. 4.

### 3.2.3 Standard model v. analytical model

Applying standard tropospheric chemistry to the inlet yields the expected behavior of equal yields of H$_2$SO$_4$ from HO$_2$ and CH$_3$O$_2$ radicals at small [NO]/[O$_2$] ($\alpha = 1$), and small yields of H$_2$SO$_4$ for RO$_2$ relative to HO$_2$ at large [NO]/[O$_2$]

($\alpha \to 0$). This standard model was presented in Edwards et al. (2003), and is shown in Fig. 3a. It can be seen that the observations of $\alpha_{CH_3O_2}$ differ significantly from the standard model for the very lowest [NO]/[O$_2$] and, unexpectedly, values greater than unity were measured. This implies that processes dependent on both the inlet [NO]/[O$_2$] ratio (Fig. 3a) and the absolute [NO] in the inlet (Fig. 3b) are operative which produce more than one HO$_2$ per RO$_2$ for these conditions, or that H$_2$SO$_4$ is produced in addition to the conversion to HO$_2$. On the other hand, agreement between the observations and the standard model at large [NO]/[O$_2$] values is reasonable, in contrast to the results of Edwards et al. (2003) (Fig. 3a). We believe that the larger than expected α values observed by Edwards et al. (2003) were due to contaminants in the zero air used in their experiments. We found it necessary to use the cleanest synthetic air available (so-called Hydrocarbon Free, with VOC content less than 0.1 ppmV) to avoid this artifact. Edwards and colleagues did not observe the larger than unity α values at low [NO]/[O$_2$], likely because their measurements were not made at sufficiently low [NO]/[O$_2$] ratios (minimum ratio of 2.8×10^{-5}).

What reactants could convert SO$_2$ into H$_2$SO$_4$ and/or RO$_2$ into HO$_2$ with yields leading to apparent α values greater than unity at low [NO]/[O$_2$], while maintaining the inefficient conversion at high [NO]/[O$_2$]? Possible candidates are RO$_2$ and RO, or unknown chemistry involving OH and/or HO$_2$. RO would seem reasonable by analogy with OH. RO$_2$ is unlikely, although several papers in the literature discuss the oxidation of SO$_2$ by CH$_3$O$_2$ (e.g. Kan et al., 1981 and references therein). Current thinking is that the direct oxidation of SO$_2$ is quite slow ($<10^{-16}$ cm^3 molecule^{-1} s^{-1}, Sander and Watson, 1981). Kan et al. (1981), on the other hand, argue for a multiple-step mechanism involving two equilibria, which results in the oxidation of SO$_2$ while preserving the CH$_3$O$_2$ radicals. While reactions such as these might not be important in the troposphere, they could be operative in the high SO$_2$ and NO concentrations within the instrument inlet.

Yields of HO$_2$ and H$_2$SO$_4$ from the reactions of RO$_2$ radicals within the instrument inlet were calculated in the following way, and compared with the laboratory measured values. Each RO$_2$ precursor reacts with OH to produce one or more isomers. The yields of these isomers have been reported in the literature for some reactants, and structure activity relationships have been developed to predict the isomer yields (Calvert et al., 2008; Kwok and Atkinson, 1995; Neeb, 2000). We used the method of Calvert et al. (2008) for the alkane precursors, and that of Neeb for the others. Several reactions between the radicals and the reagent gases within the inlet are part of standard tropospheric chemistry, including Reaction (R1) through Reaction (R4), and the following:

$$RO + M \longrightarrow R'\cdot + R''CHO \qquad (R17)$$

$$RO \longrightarrow HO-R\cdot + O_2 + M \longrightarrow HO-RO_2 + M. \qquad (R18)$$
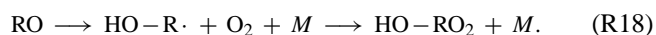
Following isomerization Reaction (R18) or decomposition Reaction (R17), the alkyl radical adds to O$_2$ to form a new organic peroxy radical, which cascades through the sequence. When produced, HO$_2$ reacts as described earlier. Using the above chemistry, we found it not possible to explain our laboratory observations of the sensitivity of RO$_2$ radicals in our instrument for the lowest [NO]/[O$_2$] ratios. Missing from this chemistry are peroxy and alkoxy radicals reactions with SO$_2$. Although not recognized as relevant to tropospheric chemistry, based on analogy with OH and HO$_2$, one might speculate that RO would react with SO$_2$ leading to SO$_3$ and other products. Edwards et al. (2003) proposed a reaction between CH$_3$O and SO$_2$ to explain their observation of higher than expected H$_2$SO$_4$ yields at high [NO]/[O$_2$] ratios. No detailed mechanism was proposed, other than to indicate that H$_2$SO$_4$ was eventually produced along with other non-radical or slowly-reacting products.

Kan et al. (1981) reported results of detailed laboratory chamber studies of the kinetics and mechanism of reactions between CH$_3$O$_2$, CH$_3$O and CH$_3$ with SO$_2$ in the presence of O$_2$ and NO. They argue that these reactions involve multiple equilibria between the radicals, SO$_2$ and O$_2$. They also explain that conventional flow tube kinetics studies do not observe a reaction between CH$_3$O$_2$ and SO$_2$ due to the absence of O$_2$, resulting in the recommended (Sander et al., 2006) rate coefficient for CH$_3$O$_2$ + SO$_2$ at an upper limit of 5×10^{-17} cm^3 molecule^{-1} s^{-1}. This is discussed in a footnote in Sander et al. (2006), with the conclusion that the decomposition of the CH$_3$O$_2$SO$_2$ adduct back to CH$_3$O$_2$ and SO$_2$ likely dominates under atmospheric conditions. While this may be true, we seek a mechanism for the production of additional HO$_2$ and/or H$_2$SO$_4$ in our instrument inlet. We hypothesize that there are three potential mechanisms that produce H$_2$SO$_4$ without consumption of radicals. Mechanism (a) involves the reaction between RO$_2$ and SO$_2$ along the lines discussed by Kan et al. (1981)

$$RO_2 + SO_2 + M \longrightarrow RO_2SO_2 + M \qquad (R19)$$

$$RO_2SO_2 + O_2 + M \longrightarrow RO_2SO_2O_2 + M \qquad (R20)$$
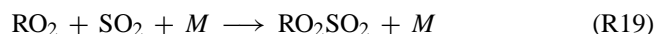
The RO$_2$SO$_2$O$_2$ behaves like any other peroxy radical, primarily reacting with NO in our inlet.

$$RO_2SO_2O_2 + NO \longrightarrow RO_2SO_2O + NO_2 \qquad (R21)$$
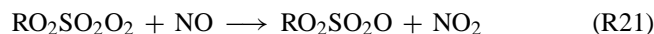
The alkoxy radical produced could potentially undergo a number of reactions, but decomposition is most likely.

$$RO_2SO_2O \longrightarrow RO_2 + SO_3 \qquad (R22)$$
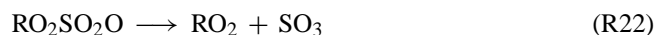
This mechanism produces SO$_3$ and eventually H$_2$SO$_4$ without consumption of radicals, and has the potential to explain our laboratory measurements. Overall, the reaction involves the catalytic oxidation of SO$_2$ to SO$_3$.
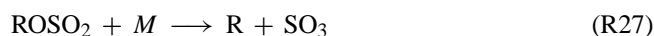
$$RO_2 + SO_2 + O_2 + NO \longrightarrow RO_2 + SO_3 + NO_2 \qquad (R23)$$
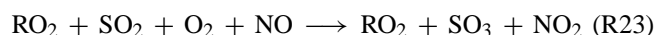
Mechanism (b), also discussed by Kan et al. (1981), involves the reaction between RO and SO$_2$ resulting in production of RO and SO$_3$. The chemistry is similar to that shown for RO$_2$ + SO$_2$, with the final reaction involving the decomposition of ROSO$_2$O into RO and SO$_3$ and an overall reaction:

$$RO + SO_2 + O_2 + NO \longrightarrow RO + SO_3 + NO_2 \quad \text{(R24)}$$
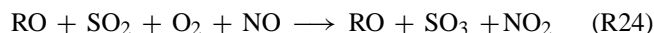
Mechanism (c) involves reaction between RO and SO$_2$ leading to RO$_2$ and SO$_3$. This is only slightly different than mechanism (b), but will lead to lower yields when the nitrate yield in the reaction of RO$_2$ with NO is significant.

$$RO + SO_2 + M \longrightarrow ROSO_2 + M \quad \text{(R25)}$$

$$ROSO_2 + O_2 \longrightarrow RO_2 + SO_3 \quad \text{(R26)}$$

$$ROSO_2 + M \longrightarrow R + SO_3 \quad \text{(R27)}$$

$$R + O_2 + M \longrightarrow RO_2 + M \quad \text{(R28)}$$

Overall, this mechanism converts RO and SO$_2$ into RO$_2$ and SO$_3$.

$$RO + SO_2 + O_2 \longrightarrow RO_2 + SO_3 \quad \text{(R29)}$$
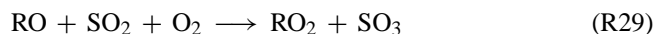
The rate laws for each of these mechanisms are similar, if we assume that the reaction of the sulfur containing peroxy radical with NO is not rate limiting. In that case, the production rate of SO$_3$ is given by the following.

$$\left(\frac{d[SO_3]}{dt} \right)_a = k_a \, [O_2] \, [SO_2] \, [RO_2] \quad \text{(4)}$$

where k_a is the effective rate coefficient for the overall process.

Similar equations apply to mechanisms (b) and (c). Equations for the production of HO$_2$ from Reactions (R1–R7), and mechanisms (a), (b) and (c) were derived and used to predict the yield of H$_2$SO$_4$ from RO$_2$ relative to HO$_2$ for each of the isomers produced in the reactions of OH with the various precursors studied. The rate coefficients, k_a, k_b, and k_c were used as fit parameters. In addition, the rate coefficients for RO + NO reactions for alkanes larger than C$_3$ and the other species were allowed to vary within a range (5 × 10^{-12} to 4 × 10^{-11} cm^3 molecule^{-1} s^{-1}) as part of the fitting procedure. The rate coefficients for RO + O$_2$ were set to their recommended values (1 × 10^{-14} for primary RO and 8 × 10^{-15} for secondary RO), and to zero for tertiary RO (Atkinson, 1994, 1997; Calvert et al., 2008). In a few cases, no satisfactory fit could be found varying the four rate coefficients, and in those cases the rate coefficients for RO + O$_2$ were also fit. RO$_2$ + NO rate coefficients were set to recommended values for smaller RO$_2$ (C$_3$ and smaller alkanes), and to 8 × 10^{-12} for larger alkanes and the other species. This approach was able to reproduce the laboratory observations with remarkable accuracy.

The rate coefficients yielding the best fits for the RO + NO reactions were in the 3–4 × 10^{-11} range for C$_6$ and smaller alkanes. The C$_7$ alkane was 1 × 10^{-11}, while for the alkenes the best fit was 5 × 10^{-12}. For the aromatics, the values needed to be set at the kinetic limit of about 4 × 10^{-10}. The effective overall rate coefficient for mechanism (a) averaged approximately 1 × 10^{-31} cm^6 molecule^{-2} s^{-1}, resulting in a value of k_a[O$_2$] at low [NO]/[O$_2$] ratios of about 3 × 10^{-13} cm^3 molecule^{-1} s^{-1}, and about 5 × 10^{-14} at high [NO]/[O$_2$] ratios. These values are larger than the value recommended by Kan et al. (1981) of 1.4 × 10^{-14}. There is variability in the best values for k_a. For example, it is about 1 × 10^{-36} cm^6 molecule^{-2} s^{-1} for *tert*-butoxy radicals. Values are also similar for 2- and 3-heptylperoxy radicals. Some best fit values are zero (e.g. for 2- and 3-hexylperoxy, and many of the tertiary peroxy radicals) while the value for 1-hexylperoxy is unrealistically large (2 × 10^{-26} cm^6 molecule^{-2} s^{-1}). This is likely an artifact of the fitting procedure. Rate coefficients for mechanism (b) range from 10^{-31} to 10^{-27} cm^6 molecule^{-2} s^{-1} with the straight-chained peroxy radicals tending to have the higher values. Tertiary peroxy radicals often have zero values. The radicals derived from alkenes are generally at the low end, mostly between 2 × 10^{-31} and 10^{-29} cm^6 molecule^{-2} s^{-1}. Finally, the rate coefficients for mechanism (c) range from 10^{-32} to 10^{-29} cm^6 molecule^{-2} s^{-1}. Values are zero for isoprene and the aromatics, and mid-10^{-32} for the other alkenes. Overall, for most peroxy radicals, mechanism (a) accounts for most of the effect of increasing the yield of H$_2$SO$_4$ from RO$_2$ in our inlet. Mechanism (b) seems to more important for alkenes – along with (a), and (c) only has an impact for a few specific isomers (e.g. 2- and 3-hexylperoxy and 4-heptylperoxy). The revised inlet chemistry for RO$_2$ and HO$_2$ in the PeRCIMS inlet based on this fit is shown in Schemes 1 and 2. We clearly need more kinetic data to constrain these mechanisms, but it appears that the reactions between RO$_2$ and RO with SO$_2$ in the presence of O$_2$ and NO are operative in our inlet and contribute significantly to the signals we observe. It is our intent to study this chemistry further and in a future paper to examine its impacts in the atmosphere.

4   Ambient measurements

For ambient peroxy radical measurements, a fraction of the signal measured in the HO$_2$ mode is due to RO$_2$ radicals. The actual HO$_2$ concentration, [HO$_2$]$_{amb}$, in an individual HO$_2$-mode measurement can be approximated using the previous and subsequent measurements in the HO$_2$ + RO$_2$ mode. Likewise, the actual concentration of HO$_2$ + RO$_2$ in an individual HO$_2$ + RO$_2$-mode measurement can be approximated using previous and subsequent measurements in the HO$_2$ mode. Ambient HO$_2$ and RO$_2$ concentrations are thus determined using the following:

$$[HO_2]_{amb} = S_{low} F_{low} - \alpha_{low} \left[\frac{S_{low} F_{low} - S_{high} F_{high}}{\alpha_{low} - \alpha_{high}} \right] \quad (5)$$

$$[RO_2]_{amb} = \frac{S_{low} F_{low} - S_{high} F_{high}}{\alpha_{low} - \alpha_{high}} \quad (6)$$

The term S_{low} is equal to $S_{HO_2,low} + S_{RO_2,low}$, the sum of the signals due to HO$_2$ and RO$_2$ in the HO$_2$ + RO$_2$ mode or low [NO]/[O$_2$]. Likewise S_{high} is equal to $S_{HO_2,high} + S_{RO_2,high}$, the sum of the signals due to HO$_2$ and RO$_2$ in the HO$_2$ mode or high [NO]/[O$_2$] mode. The terms F_{low} and F_{high} are the calibration factors for the HO$_2$ + RO$_2$ and HO$_2$ modes, respectively, and are defined as:

$$F_{low} = [HO_2]_{H_2} \big/ S_{H_2,low} \quad (7)$$

$$F_{high} = [HO_2]_{H_2} \big/ S_{H_2,high} \quad (8)$$

From Eq. (2), the absolute concentration of HO$_2$, $[HO_2]_{H_2}$, in both modes is $2It\sigma_{H_2O}\phi_{H_2O}[H_2O]$. Finally, α_{high} and α_{low} are the measurement sensitivities to RO$_2$ (relative to HO$_2$) at the two ambient measurement modes with high [NO]/[O$_2$] and low [NO]/[O$_2$] and are defined as:

$$\alpha_{high} = \frac{S_{RO_2,high}}{S_{HO_2,high}} \quad (9)$$

$$\alpha_{low} = \frac{S_{RO_2,low}}{S_{HO_2,low}}. \quad (10)$$

The values of F_{low}, F_{high}, α_{high} and α_{low} are determined during laboratory instrument characterizations and absolute calibration measurements.

Because the ambient concentration of RO$_2$ is not measured independently from HO$_2$, it is subject to greater uncertainty as it relies on the difference of two measured signals. Thus, we recommend that ambient data are reported as HO$_2$ and HO$_2$ + RO$_2$ concentrations, such that reported HO$_2$ + RO$_2$ concentrations are the combination of both [HO$_2$] and [RO$_2$], and are essentially the HO$_2$ + RO$_2$-mode signal with a small correction:

$$[HO_2 + RO_2]_{amb} \quad (11)$$

$$= S_{low} F_{low} + \frac{(1 - \alpha_{low})(S_{low} F_{low} - S_{high} F_{high})}{\alpha_{low} - \alpha_{high}}$$

which can be simplified to:

$$[HO_2 + RO_2]_{amb} \quad (12)$$

$$= \frac{S_{low} F_{low} (1 - \alpha_{high}) - S_{high} F_{high} (1 - \alpha_{low})}{\alpha_{low} - \alpha_{high}}$$

Thus, both [HO$_2$]$_{amb}$ and [HO$_2$ + RO$_2$]$_{amb}$ are determined using the signals measured during both the HO$_2$ and the HO$_2$ + RO$_2$ modes, and the α values for each mode. For this reason, for each HO$_2$ mode measurement, [HO$_2$]$_{amb}$ is calculated using the average of the previous and following

signal measurements in the HO$_2$ + RO$_2$ mode, $S_{low,ave}$, and likewise, [HO$_2$ + RO$_2$]$_{amb}$ is calculated using the average of the previous and following signal measurements in the HO$_2$ mode, $S_{high,ave}$.

Uncertainties of ambient measurements arise from a combination of uncertainties in a number of factors including calibration, counting statistics, and flow controller and pressure transducer accuracy, as discussed by Edwards et al. (2003). Present PeRCIMS uncertainties associated with actinometry and calibrations are identical to those shown by Edwards et al., while estimated uncertainties of the HSO$_4^-$ counting statistics in ambient measurements are now both 10% for signals well above the detection limit. This leads to a 95% confidence interval of typically $\pm35\%$ for ambient measurements of both [HO$_2$] and [HO$_2$ + RO$_2$].

4.1 Ambient data from the MIRAGE and INTEX-B campaigns

In Spring 2006, the PeRCIMS instrument was deployed on the NSF/NCAR C-130 during the MIRAGE-Mex and NASA INTEX-B field campaigns, described in detail in an overview paper (Singh et al., 2009). The MIRAGE-Mex (Megacities Impact on Regional and Global Environment-Mexico City) campaign, which took place in March 2006, was designed to investigate the chemical and physical transformation of gases and aerosol in the polluted outflow from Mexico City. INTEX-B, the second phase of NASA's Intercontinental Transport Experiment which took place during April–May 2006, was designed to quantify the transpacific transport and evolution of Asian pollution to North America. Concentrations of NO were also measured on the C-130 by chemiluminescence (Ridley et al., 2004). Following the field studies, the NASA Langley time-dependent photochemical box model (Crawford et al., 1999; Olson et al., 2001, 2006; Fried et al., 2008a,b) was used to estimate radical concentrations along the flight tracks of a number of the C-130 flights, constrained by observations of other chemical species made onboard the aircraft.

Shown in Fig. 9 is a time-series plot of a segment of the C-130 flight on 10 March 2006. Observations of HO$_2$ and HO$_2$ + RO$_2$ mixing ratios are shown on the lower plot, along with modeled HO$_2$, CH$_3$O$_2$ and non-CH$_3$O$_2$ RO$_2$, while the upper plot shows the corresponding GPS altitude, 1-Hz [NO] observations and 1-min averaged [NO]. Both plots are highlighted in green where the 1-min average [NO] is above 0.5 ppbV. The observations and model output are generally in good agreement, but under certain conditions the measured and modeled peroxy radical concentrations deviate significantly and systematically. For example, when [NO] > 0.5 ppbV, (both 1-Hz and 1-min averaged [NO]) the model-predicted HO$_2$ + RO$_2$ mixing ratios are much lower than the actual observed radical concentrations, and to a lesser extent, the model-predicted HO$_2$ mixing ratios are lower than the observed data. This tendency
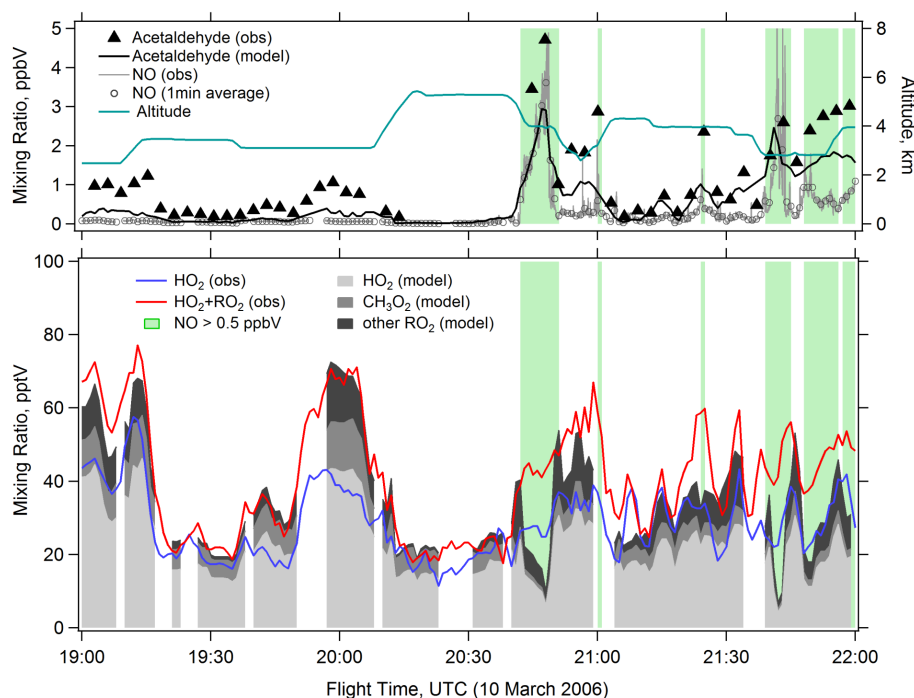
Fig. 9. Time-series plot of the observed and modeled acetaldehyde (top panel) and peroxy radicals (bottom panel) during a section of the flight on 10 March 2006. Local time in the flight region is UTC-6 h. Grey areas defined in the legend on the lower plot are stacked modeled [HO$_2$], [CH$_3$O$_2$] and non-CH$_3$O$_2$ [RO$_2$]. The 1-s [NO] and 1-min [NO] are both included on the top panel, along with altitude. Time periods when the 1-min average [NO] is greater than 0.5 ppbV are highlighted in green on both plots.

for the measurement/model ratio to increase with increasing NO$_x$ has been discussed previously for measurements of hydroperoxy radicals and hydroxyl radicals (Faloona et al., 2000; Ren et al., 2005, 2006; Olson et al., 2006), and for this reason we consider times when [NO] < 0.5 ppbV in the following analysis. The discrepancy between measurements and model with high NO$_x$ for the peroxy radical data from MIRAGE-Mex, INTEX-B and other more recent campaigns will be explored further in a separate paper. Other times the observations and model differed significantly during the 2006 campaigns occurred both when the C-130 was in air masses heavily influenced by biomass burning, and in the marine boundary layer.

Overall, there were six C-130 MIRAGE-Mex flights and eight INTEX-B flights with both observations and box model peroxy radical data available for comparison. In total, there were approximately 2700 HO$_2$ and 3000 HO$_2$ + RO$_2$ data points with both ambient and model values. Excluding data points with measured or modeled peroxy mixing ratios < 2 pptV (parts per trillion by volume) to eliminate extreme concentration ratios, as well as those with corresponding 1-min average [NO] > 0.5 ppbV, there are approximately 2500 HO$_2$ and 2800 HO$_2$ + RO$_2$ data points remaining for comparison. From these, the mean measurement/model ratios for the MIRAGE-Mex flights were 1.25 ± 0.74 (HO$_2$) and 1.54 ± 0.73 (HO$_2$ + RO$_2$), and for the INTEX flights,

1.15 ± 0.58 (HO$_2$) and 1.36 ± 0.77 (HO$_2$ + RO$_2$), all 1 σ standard deviation.

Both of these data sets will be thoroughly explored in separate papers. In general, however, the observations tend to be larger than the box model predicts, with more deviation between measurement and model during the MIRAGE-Mex campaign. The observations of [HO$_2$] and [HO$_2$ + RO$_2$] during these campaigns demonstrate that we are able to measure separated hydroperoxy and organic peroxy radical concentrations on timescales relevant for fast photochemistry and useful for comparison to photochemical box models of aircraft observations.

4.2 Impact of alpha value uncertainties

The reported $\alpha_{\text{high,CH}_3\text{O}_2}$ and $\alpha_{\text{low,CH}_3\text{O}_2}$ values for the HO$_2$ and HO$_2$ + RO$_2$ measurement modes are 0.17 ± 0.04 and 1.22 ± 0.08. To determine the impact of the alpha value uncertainties, we used the data set from the MIRAGE-Mex flight on 10 March. By changing the α_{high} value by ±25% (the estimated uncertainty), the individual calculated [HO$_2$] changed by less than 3% on average. The calculated [HO$_2$ + RO$_2$] changed by less than 1%. Similarly, by changing the α_{low} value by ±7%, the calculated [HO$_2$] and [HO$_2$ + RO$_2$] change by less than 1% and 2%, on average,
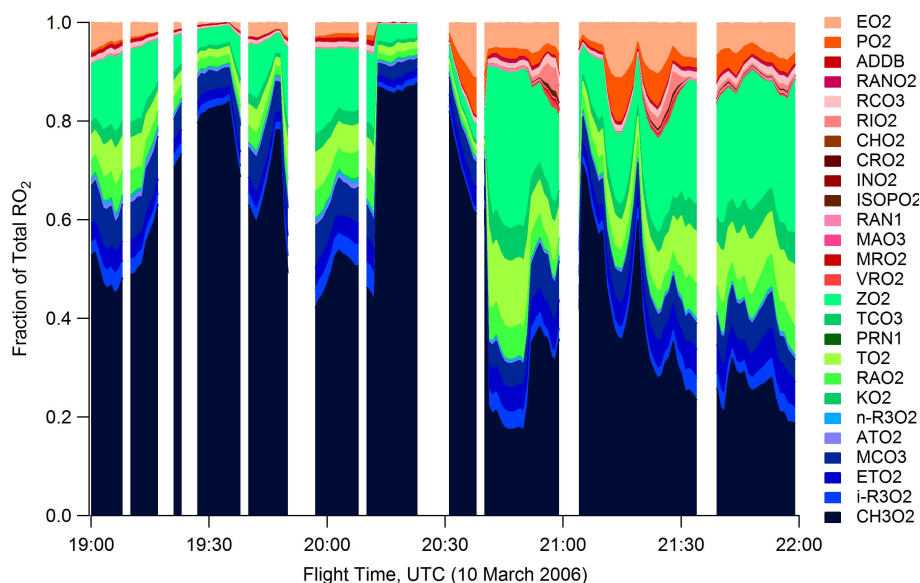
Fig. 10. Time-series plot of modeled RO_2 groups as a fraction of the total RO_2 for the flight on 10 March 2006. Blue-toned groups are those that are primarily measured in the $HO_2 + RO_2$ mode and not in the HO_2 mode, red-toned groups are those that are likely measured in the HO_2 mode, and green-toned groups are those that contain a mixture of RO_2 that generate signals in the HO_2 and the $HO_2 + RO_2$ modes. A full description of the RO_2 groups is in Table 6.

respectively. These changes are all well within the reported peroxy radical measurement uncertainties of $\pm 35\%$.

What the reported $\alpha_{CH_3O_2}$ uncertainties do not account for directly account, however, is the impact on α_{high} and α_{low} due to organic peroxy radicals other than CH_3O_2. As shown in Fig. 8a–c, the $[NO]/[O_2]$ dependence of α_{RO_2} values for some RO_2 precursors can vary significantly from that of methane. For this reason, it is important to consider the impact that RO_2 precursor speciation can have on the uncertainty of both calculated HO_2 and $HO_2 + RO_2$ concentrations.

To estimate the impact of non-CH_3O_2 RO_2 on the uncertainties of the reported $[HO_2]$ and $[HO_2 + RO_2]$ in the MIRAGE-Mex and INTEX-B data sets, we assessed the RO_2 precursor loading for different types of air masses measured during a MIRAGE-Mex flight, and looked at the measurement/model ratios with respect to the box modeled fraction of total RO_2 that is CH_3O_2 for both campaigns full data sets.

During the 10 March flight, the C-130 sampled air masses with a variety of RO_2 precursors at a wide range of relative concentrations. The NASA Langley Research Center (LaRC) box model output for the non-CH_3O_2 RO_2 along the flight track is the sum of 25 parameterized RO_2 groups based on precursor type and oxidant. The chemical scheme for NMHC in the box model derives from that in the lumped scheme of Lurmann et al. (1986), with updates as described in Crawford et al. (1999) and Olson et al. (2006). The 25 functional peroxy groups are described in Table 6. Figure 10 is a plot of the 25 RO_2 groups and CH_3O_2 as a fraction of the total RO_2 according to the model for the same time period shown in Fig. 9. During the flight, the CH_3O_2

fraction is predicted to range from 16% to 92% of the total RO_2. Based on the experiments with NMHC RO_2 precursors, the PeRCIMS inlet is not sensitive to all RO_2 species equally. As well, there are a number of RO_2 radicals that are converted into HO_2 in the HO_2 mode, and are thus included in the observed $[HO_2]$. The 25 RO_2 groups in Fig. 10 have been colored according to the sensitivity of the PeRCIMS measurement: blue-toned groups are those that are primarily observed in the RO_2 mode, red-toned groups are those that primarily generate a signal in the HO_2 mode (e.g., from alkene precursors), and the green-toned groups contain a mixture of RO_2 radicals that may be observed as RO_2 or HO_2.

From Fig. 10, at some points during the flight, as much as 50% of the ambient RO_2 could be measured in the HO_2 mode. Thus, although observed $[HO_2 + RO_2]$ should not be impacted, this implies that observed $[HO_2]$ would be greater than the modeled $[HO_2]$ in regions where the non-CH_3O_2 RO_2 fraction is high. From Fig. 9, although there are a few occasions when the observed $[HO_2]$ is significantly greater than the modeled $[HO_2]$, the majority of these times coincide with the observed $[HO_2 + RO_2]$ significantly exceeding that of the model. This suggests there are RO_2 and/or RO_2 precursors that are not being accounted for in the model or by the VOC measurements, either in the gas or the aerosol phase. Because of the possibility of some non-CH_3O_2 RO_2 being observed in the HO_2 mode, the reported uncertainties of measured $[HO_2]$ are larger in regions where non-CH_3O_2 RO_2/CH_3O_2 is large (>0.5), as observed HO_2 is systematically high.

Table 6. Parameterized box model RO$_2$ groups comprising the non-CH$_3$O$_2$ RO$_2$.

RO$_2$ group	Product of Reaction	RO$_2$ structure	PeRCIMS sensitive to RO$_2$ group*
ETO2	ethane + OH	C$_2$H$_5$O$_2$	yes
n-R3O2	propane + OH	n-C$_3$H$_7$O$_2$	yes
i-R3O2	propane + OH	i-C$_3$H$_7$O$_2$	yes
RAO2	lumped C$_{4+}$ alkanes + OH	various C$_n$H$_{2n+1}$O$_2$	partial
EO2	ethene + OH	HOCH$_2$CH$_2$O$_2$	as HO$_2$
PO2	propene + OH	HOC$_3$H$_6$O$_2$	as HO$_2$
CHO2	lumped alkenes + O$_3$	various	as HO$_2$
CRO2	lumped alkenes + O$_3$	various	as HO$_2$
PRN1	lumped alkenes + NO$_3$	various	partial
ADDB	benzene + OH	C$_6$H$_6$(OH)O$_2$	as HO$_2$
TO2	C$_{7+}$ aromatics + OH	various	partial
RIO2	isoprene + OH	various	as HO$_2$
VRO2	MVK + OH	various	as HO$_2$
MRO2	methacrolein + OH	methacrolein RO$_2$	as HO$_2$
INO2	isoprene + NO$_3$	various	as HO$_2$
ISOPO2	lumped isoprene products + OH	various	as HO$_2$
ATO2	acetone + OH	CH$_3$COCH$_2$O$_2$	yes
KO2	MEK (methyl ethyl ketone) + OH	MEK RO$_2$	very likely
MCO3	various	CH$_3$CO$_3$	yes
RCO3	associated with PPN (C$_2$H$_5$CO$_3$NO$_2$)	various	as HO$_2$
TCO3	decomposition of CHOCH=CHCO$_3$NO$_2$	CHOCH=CH$_3$O$_3$	partial
ZO2	lumped aromatic RO$_2$	various	partial
MAO3	decomposition of MPAN (from methacrolein)	CH$_2$=C(CH$_3$)CO$_3$	as HO$_2$
RAN1	lumped C$_{4+}$ alkyl nitrates + OH	various	as HO$_2$
RANO2	lumped RAN1 + NO	various	as HO$_2$

* Sensitivity of PeRCIMS instrument to RO$_2$ group: "yes" implies RO$_2$ in group will be observed in the HO$_2$ + RO$_2$ mode, "partial" implies some RO$_2$ in group will be observed in the HO$_2$ + RO$_2$ mode, "as HO$_2$" implies RO$_2$ are most likely observed in the HO$_2$ mode, and "very likely" implies that although these RO$_2$ have not been studied, it is expected that the RO$_2$ will be observed in the HO$_2$ + RO$_2$ mode.

It is possible that some of the observed RO$_2$ that is not accounted for by the box model is a product of the OH-oxidation of acetaldehyde, CH$_3$CO$_3$. According to Apel et al. (2010), the two VOCs with the greatest influence on OH reactivity in the Mexico City Metropolitan Area (MCMA) region are acetaldehyde and formaldehyde. The NASA LaRC box model is not constrained by acetaldehyde observations, and the model-predicted acetaldehyde concentrations are on average half the observed [acetaldehyde] measured onboard the C-130 by the NCAR Trace Organic Gas Analyzer (TOGA) instrument while it was in the region of the MCMA during the 10 March flight (Fig. 9, top panel). During this time, approximately 20:30–23:20 UTC, the observed [HO$_2$ + RO$_2$] was higher than the modeled [HO$_2$ + RO$_2$]. The PeRCIMS is sensitive to CH$_3$CO$_3$ as RO$_2$ (MCO3 in Table 6), so it is possible that lower predicted acetaldehyde concentrations contribute to the modeled [HO$_2$ + RO$_2$] being lower than the observed [HO$_2$ + RO$_2$]. However, this is likely only a part of the overall RO$_2$ signal missing from the

model, as doubling the MCO3 contribution in Fig. 10 would not account for a significant increase in modeled RO$_2$.

5 Conclusions

An improved method for separating and measuring hydroperoxy and organic peroxy radicals has been developed and characterized extensively for both ground-based and airborne measurements. The method builds upon previously described CIMS techniques for measuring peroxy radicals in that both HO$_2$ and HO$_2$ + RO$_2$ modes can be observed each minute, with improved separation between modes.

Operationally, the use of NO and SO$_2$ mixtures that can be used in both measurement modes by simply increasing or decreasing the flow rates by a factor of 4.5 has allowed for significantly faster switching between measurement modes than previously possible with pure reagent gases. By diluting the sample 1:1 with diluent gases, the overall measurement sensitivity has been effectively halved. However, compared to

the fourfold dilution used by Hanke et al. (2002), this method allows for a higher degree of sensitivity by only diluting the sample flow by half and combining the dilution with two inlet NO mixing ratios. Most importantly, because α_{RO_2} in the HO$_2$ mode is only ≈ 0.2 for CH$_3$O$_2$, CH$_3$CH$_2$O$_2$ and other simple organic peroxy radicals, we are able to successfully separate HO$_2$ and RO$_2$ for the majority of atmospheric conditions over a wide range of RO$_2$ precursor concentrations and mixtures. Undermeasurement of [RO$_2$] and overmeasurement of [HO$_2$] due to conversion in the inlet in the HO$_2$ mode may occur in regions where unsaturated hydrocarbons are present in high concentrations. For this reason, the reported [HO$_2$] uncertainty will be larger in these regions. However, the observed [RO$_2$] during a MIRAGE-Mex flight are on average higher than the model predicts in these circumstances, indicating that there are likely additional sources of RO$_2$ that are not being accounted for in the model.

Edited by: J. Stutz

References

Apel, E. C., Emmons, L. K., Karl, T., Flocke, F., Hills, A. J., Madronich, S., Lee-Taylor, J., Fried, A., Weibring, P., Walega, J., Richter, D., Tie, X., Mauldin, L., Campos, T., Weinheimer, A., Knapp, D., Sive, B., Kleinman, L., Springston, S., Zaveri, R., Ortega, J., Voss, P., Blake, D., Baker, A., Warneke, C., Welsh-Bon, D., de Gouw, J., Zheng, J., Zhang, R., Rudolph, J., Junkermann, W., and Riemer, D. D.: Chemical evolution of volatile organic compounds in the outflow of the Mexico City Metropolitan area, Atmos. Chem. Phys., 10, 2353–2375, doi:10.5194/acp-10-2353-2010, 2010.

Atkinson, R.: Gas-phase tropospheric chemistry of organic compounds, J. Phys. Chem. Ref. Data, 2, 1–216, 1994.

Atkinson, R.: Gas-phase tropospheric chemistry of volatile organic compounds, 1. Alkanes and alkenes, J. Phys. Chem. Ref. Data, 26, 215–290, doi:10.1063/1.556012, 1997.

Atkinson, R.: Atmospheric chemistry of VOCs and NO$_x$, Atmos. Environ., 34, 2063–2101, doi:10.1016/S1352-2310(99)00460-4, 2000.

Atkinson, R. and Arey, J.: Atmospheric degredation of volatile organic compounds, Chem. Rev., 103, 4605–4638, doi:10.1021/cr0206420, 2003.

Atkinson, R.: Rate constants for the atmospheric reactions of alkoxy radicals: An updated estimation method, Atmos. Environ., 41, 8468–8485, doi:10.1016/j.atmosenv.2007.07.002, 2007.

Blitz, M., Pilling, M. J., Robertson, S. H., and Seakins, P. W.: Direct studies on the decomposition of the *tert*-butoxy radical and its reaction with NO, Phys. Chem. Chem. Phys., 1, 73–80, doi:10.1039/A806524A, 1999.

Brasseur, G. P., Orlando, J. J., and Tyndall, G. S.: Nitrogen Compounds, in: Atmospheric Chemistry and Global Change, Oxford University Press, New York, 235–289, 1999.

Calvert, J. G., Derwent, R. G., Orlando, J. J., Tyndall, G. S., and Wallington, T. J.: Mechanisms of the Atmospheric Oxidation of the Alkanes, Oxford University Press, New York, 1008 pp., 2008.

Cantrell, C. A., Zimmer, A., and Tyndall, G. S.: Absorption cross sections for water vapor from 183 to 193 nm, Geophys. Res. Lett., 24, 2195–2198, doi:10.1029/97GL02100, 1997a.

Cantrell, C. A., Zimmer, A., and Tyndall, G. S.: Correction to "Absorption cross sections for water vapor from 183 to 193 nm", Geophys. Res. Lett., 24, 2687, doi:10.1029/97GL02803, 1997b.

Cantrell, C. A., Mauldin, L., Zondlo, M., Eisele, F., Kosciuch, E., Shetter, R., Lefer, B., Hall, S., Campos, T., Ridley, B., Walega, J., Fried, A., Wert, B., Flocke, F., Weinheimer, A., Hannigan, J., Coffey, M., Atlas, E., Stephens, S., Heikes, B., Snow, J., Blake, D., Blake, N., Katzenstein, A., Lopez, J., Browell, E. V., Dibb, J., Scheuer, E., Seid, G., and Talbot, R.: Steady state free radical budgets and ozone photochemistry during TOPSE, J. Geophys. Res., 108, 8361, doi:10.1029/2002JD002198, 2003a.

Cantrell, C. A., Edwards, G. D., Stephens, S., Mauldin, L., Kosciuch, E., Zondlo, M., and Eisele, F.: Peroxy radical observations using chemical ionization mass spectrometry during TOPSE, J. Geophys. Res., 108, 8371, doi:10.1029/2002JD002715, 2003b.

Cantrell, C. A., Edwards, G. D., Stephens, S., Mauldin, R. L., Zondlo, M. A., Kosciuch, E., Eisele, F. L., Shetter, R. E., Lefer, B. L., Hall, S., Flocke, F., Weinheimer, A., Fried, A., Apel, E., Kondo, Y., Blake, D. R., Blake, N. J., Simpson, I. J., Bandy, A. R., Thornton, D. C., Heikes, B. G., Singh, H. B., Brune, W. H., Harder, H., Martinez, M., Jacob, D. J., Avery, M. A., Barrick, J. D., Sachse, G. W., Olson, J. R., Crawford, J. H., and Clarke, A. D.: Peroxy radical behavior during the Transport and Chemical Evolution over the Pacific (TRACE-P) campaign as measured aboard the NASA P-3B aircraft, J. Geophys. Res., 108, 8797, doi:10.1029/2003JD003674, 2003c.

Crawford, J., Davis, D., Olson, J., Chen, G., Liu, S., Gregory, G., Barrick, J., Sachse, G., Sandholm, S., Heikes, B., Singh, H., and Blake, D.: Assessment of upper tropospheric HO$_x$ sources over the tropical Pacific based on NASA GTE/PEM data: Net effect on HO$_x$ and other photochemical parameters, J. Geophys. Res., 104, 16255–16273, doi:10.1029/1999JD900106, 1999.

Edwards, G. D., Cantrell, C. A., Stephens, S., Hill, B., Goyea, O., Shetter, R. E., Mauldin, R. L., Kosciuch, E., Tanner, D. J., and Eisele, F. L.: Chemical ionization mass spectrometer instrument for the measurement of tropospheric HO$_2$ and RO$_2$, Anal. Chem., 75, 5317–5327, doi:10.1021/ac034402b, 2003.

Faloona, I., Tan, D., Brune, W. H., Jaegle, L., Jacob, D. J., Kondo, Y., Koike, M., Chatfield, R., Pueschel, R., Ferry, G., Sachse, G., Vay, S., Anderson, B., Hannon, J., and Fuelberg, H.: Observations of HO$_x$ and its relationship with NO$_x$ in the upper troposphere during SONEX, J. Geophys. Res., 105, 3771–3783, doi:10.1029/1999JD900914, 2000.

Fried, A., Walega, J. G., Olson, J. R., Crawford, J. H., Chen, G., Weibring, P., Richter, D., Roller, C., Tittel, F. K., Heikes, B. G., Snow, J. A., Shen, H., O'Sullivan, D. W., Porter, M., Fuelberg, H., Halland, J., and Millet, D. B.: Formaldehyde over North America and the North Atlantic during the summer 2004 INTEX campaign: Methods, observed distributions, and measurement-model comparisons, J. Geophys. Res., 113, D10302, doi:10.1029/2007JD009760, 2008a.

Fried, A., Olson, J. R., Walega, J. G., Crawford, J. H., Chen, G., Weibring, P., Richter, D., Roller, C., Tittel, F., Porter, M., Fuelberg, H., Halland, J., Bertram, T. H., Cohen, R. C., Pickering, K., Heikes, B. G., Snow, J. A., Shen, H., O'Sullivan, D. W., Brune, W. H., Ren, X., Blake, D. R., Blake, N., Sachse, G., Diskin, G. S., Podolske, J., Vay, S. A., Shetter, R. E., Hall, S. R., Anderson, B. E., Thornhill, L., Clarke, A. D., McNaughton, C. S., Singh, H. B., Avery, M. A., Huey, G., Kim, S., and Millet, D. B.: Role of convection in redistributing formaldehyde to the upper troposphere over North America and the North Atlantic during the summer 2004 INTEX campaign, J. Geophys. Res., 113, D17306, doi:10.1029/2007JD009760, 2008b.

Fuchs, H., Holland, F., and Hofzumahaus, A.: Measurement of tropospheric RO$_2$ and HO$_2$ radicals by a laser-induced fluorescence instrument, Rev. Sci. Instrum., 79, 084104, doi:10.1063/1.2968712, 2008.

Green, D. W. and Perry, R. H.: Perry's Chemical Engineers' Handbook, 8th Edition, McGraw-Hill, United States, 2400 pp., 2007.

Green, T. J., Reeves, C. E., Fleming, Z. L., Brough, N., Richard, A. R., Bandy, B. J., Monks, P. S., Penkett, S. A.: An improved dual channel PERCA instrument for atmospheric measurements of peroxy radicals, J. Environ. Monitor., 8, 530–536, doi:10.1039/b514630e, 2006.

Hanke, M., Uecker, J., Reiner, T., and Arnold, F.: Atmospheric peroxy radicals: ROXMAS, a new mass-spectrometric methodology for speciated measurements of HO$_2$ and ΣRO$_2$ and first results, Int. J. Mass Spectrom., 213, 91–99, 2002.

Hasson, A. S., Chung, M. Y., Kuwata, K. T., Converse, A. D., Krohn, D., and Paulson, S. E.: Reaction of Criegee intermediates with water vapor - An additional source of OH radicals in alkene ozonolysis, J. Phys. Chem. A, 107, 32, 6176–6182, doi:10.1021/jp0346007, 2003.

Heard, D. E. and Pilling, M. J.: Measurement of OH and HO$_2$ in the troposphere, Chem. Rev., 103, 5163–5198, doi:10.1021/cr020522s, 2003.

Kan, C. S., Calvert, J. G., and Shaw, J. H.: Oxidation of sulfurdioxide by methylperoxy radicals, J. Phys. Chem., 85, 1126–1132, doi:10.1021/j150609a011, 1981.

Kwok, E. S. C. and Atkinson, R.: Estimation of hydroxyl radical reaction rate constants for gas-phase organic compounds using a structure-reactivity relationship: an update, Atmos. Environ., 29, 1685–1695, doi:10.1016/1352-2310(95)00069-B, 1995.

Lotz, C. and Zellner, R.: Fluorescence excitation spectrum of the *tert*-butoxy radical and kinetics of its reactions with NO and NO$_2$, Phys. Chem. Chem. Phys., 2, 2353–2360, doi:10.1039/B001585G, 2000.

Lurmann, F. W., Lloyd, A. C., and Atkinson, R.: A chemical mechanism for use in long-range transport/acid deposition computer modeling, J. Geophy. Res., 91(D10), 10905–10936, doi:10.1029/JD091iD10p10905, 1986.

Neeb, P.: Structure-reactivity based estimation of the rate constants for hydroxyl radical reactions with hydrocarbons, J. Atmos. Chem., 35, 295–315, doi:10.1023/A:1006278410328, 2000.

Olson, J. R., Crawford, J. H., Davis, D. D., Chen, G., Avery, M. A., Barrick, J. D. W., Sachse, G. W., Vay, S. A., Sandholm, S. T., Tan, D., Brune, W. H., Faloona, I. C., Heikes, B. G., Shetter, R. E., Lefer, B. L., Singh, H. B., Talbot, R. W., and Blake, D. R.: Seasonal differences in the photochemistry of the South Pacific: A comparison of observations and model results from PEM-Tropics A and B, J. Geophys. Res., 106, 32749–32766, doi:10.1029/2001JD900077, 2001.

Olson, J. R., Crawford, J. H., Chen, G., Brune, W. H., Faloona, I. C., Tan, D., Harder, H., and Martinez, M.: A reevaluation of airborne HO$_x$ observations from NASA field campaigns, J. Geophys. Res., 111, D10301, doi:10.1029/2005JD006617, 2006.

Orlando, J. J., Tyndall, G. S., Apel, E. C., Riemer, D. D., and Paulson, S. E.: Rate coefficients and mechanisms of the reaction of Cl-atoms with a series of unsaturated hydrocarbons under atmospheric conditions, Int. J. Chem. Kinet., 35, 334–353, doi:10.1002/kin.10135, 2003.

Ren, X. R., Brune, W. H., Cantrell, C. A., Edwards, G. D., Shirley, T., Metcalf, A. R., and Lesher, R. L.: Hydroxyl and peroxy radical chemistry in a rural area of Central Pennsylvania: Observations and model comparisons, J. Atmos. Chem., 52, 231–257, doi:10.1007/s10874-005-3651-7, 2005.

Ren, X., Brune, W. H., Mao, J., Mitchell, M. J., Lesher, R. L., Simpas, J. B., Metcalf, A. R., Schwab, J. J., Cai, C., Li, Y., Demerjian, K. L., Felton, H. D., Boynton, G., Adams, A., Perry, J., He, Y., Zhou, X., and Hou, J.: Behavior of OH and HO$_2$ in the winter atmosphere in New York City, Atmos. Environ., 40, S252-S263, doi:10.1016/j.atmosenv.2005.11.073, 2006.

Ridley, B., Ott, L., Pickering, K., Emmons, L., Montzka, D., Weinheimer, A., Knapp, D., Grahek, F., Li, L., Heymsfield, G., McGill, M., Kucera, P., Mahoney, M. J., Baumgardner, D., Schultz, M., and Brasseur, G.: Florida thunderstorms: A faucet of reactive nitrogen to the upper troposphere, J. Geophys. Res., 109, D17305, doi:10.1029/2004JD004769, 2004.

Sander, S. P. and Watson, R. T.: A kinetics study of the reaction of SO$_2$ with CH$_3$O$_2$, Chem. Phys. Lett., 77, 473–475, doi:10.1016/0009-2614(81)85188-3, 1981.

Sander, S. P., Friedl, R. R., Golden, D. M., Kurylo, M. J., Moortgat, G. K., Wine, P. H., Ravishankara, A. R., Kolb, C. E., Molina, M. J., Finlayson-Pitts, B. J., Huie, R. E., and Orkin, V. L., Chemical kinetics and photochemical data for use in atmospheric studies evaluation number 15, NASA Jet Propulsion Laboratory, 2006.

Singh, H. B., Brune, W. H., Crawford, J. H., Flocke, F., and Jacob, D. J.: Chemistry and transport of pollution over the Gulf of Mexico and the Pacific: spring 2006 INTEX-B campaign overview and first results, Atmos. Chem. Phys., 9, 2301–2318, doi:10.5194/acp-9-2301-2009, 2009.

Suh, I., Zhang, R. Y., Molina, L. T., and Molina, M. J.: Oxidation mechanism of aromatic peroxy and bicyclic radicals from OH-toluene reactions, J. Am. Chem. Soc., 125, 12655–12665, doi:10.1021/ja0350280, 2003.

Taatjes, C. A.: Time-resolved infrared absorption measurements of product formation in Cl atom reactions with alkenes and alkynes, Int. Rev. Phys. Chem., 18, 419–458, doi:10.1080/014423599229938, 1999.

Tanner, D. J. and Eisele, F. L.: Present OH measurement limits and associated uncertainties, J. Geophys. Res., 100, 2883–2892, doi:10.1029/94JD02609, 1995.

Tully, F. P., Goldsmith, J. E. M., and Droege, A. T.: Hydrogen-atom abstraction from alkanes by OH.4. Isobutane, J. Phys. Chem., 90, 5932–5937, doi:10.1021/j100280a095, 1986.

Tyndall, G. S., Cox, R. A., Granier, C., Lesclaux, R., Moortgat, G. K., Pilling, M. J., Ravishankara, A. R., and Wallington, T. J.: Atmospheric chemistry of small organic peroxy radicals, J. Geophys. Res., 106, 12157–12182, doi:10.1029/2000JD900746, 2001.